

---

Electronic Thesis and Dissertation Repository

---

9-20-2019 11:00 AM

## Height Measurement of Basil Crops for Smart Irrigation Applications in Greenhouses using Commercial Sensors

Leila Bahman  
*The University of Western Ontario*

Supervisor  
Mclsaac, Ken  
*The University of Western Ontario*

Graduate Program in Electrical and Computer Engineering  
A thesis submitted in partial fulfillment of the requirements for the degree in Master of Engineering Science  
© Leila Bahman 2019

Follow this and additional works at: <https://ir.lib.uwo.ca/etd>



Part of the [Electrical and Computer Engineering Commons](#)

---

### Recommended Citation

Bahman, Leila, "Height Measurement of Basil Crops for Smart Irrigation Applications in Greenhouses using Commercial Sensors" (2019). *Electronic Thesis and Dissertation Repository*. 6681.  
<https://ir.lib.uwo.ca/etd/6681>

This Dissertation/Thesis is brought to you for free and open access by Scholarship@Western. It has been accepted for inclusion in Electronic Thesis and Dissertation Repository by an authorized administrator of Scholarship@Western. For more information, please contact [wlsadmin@uwo.ca](mailto:wlsadmin@uwo.ca).

## Abstract

Plant height is a key phenotypic attribute that directly represents how well a plant grows. It can also be a useful parameter in computing other important features such as yield and biomass. As the number of greenhouses increase, the traditional method of measuring plant height requires more time and labor, which increases demand for developing a reliable and affordable method to perform automated height measurements of plants. This research is aimed to develop a solution to automatically measure plant height in greenhouses using low cost sensors and computer vision techniques. For this purpose, the performance of various depth sensing technologies was compared by considering the following: camera price, measurement resolution, the field of view and compatibility with the application requirements. After analyzing the alternatives, the decision was to use the Intel RealSense D435 3D Active IR Stereo Depth Camera. The algorithms developed were used to monitor plant growth of basil. Results demonstrated a promising performance of the developed system in practice.

## Keywords

Computer vision, Image processing, Plant height measurement, Plant growth analysis, Plant phenotyping, Intel RealSense depth camera, Active IR stereo, 3D plant growth, Maximum height estimation

## Summary for Lay Audience

The decision on whether to irrigate is usually an automatic process in the greenhouses. However, growers might also decide on the allocation of water to plants based on their insights and preferences. A smart irrigation system can be used to plan and schedule watering periods at least as well as an experienced grower, which in turn can potentially improve the yield and reduce costs for many greenhouses. Among growth parameters, plant height can be used to detect water stress in smart irrigation applications. Measuring height of plants manually with a measuring tape or other handheld instruments may be inaccurate, time-consuming and can easily damage plants during the measurement process. The automation of plant height measurement can make this process more efficient, accurate, and suitable for large scale trials. 3D computer vision enables computers to perceive depth in digital images and generate a three-dimensional dataset from the scene. There are many 3D sensors that can provide depth information of the scene. However, some of them cannot work properly in the greenhouses due to the complexity of the greenhouse environments and the complexity of the plant itself. This study presents an automated and non-invasive method for accurate crop plant height measurement using an Intel RealSense D435 depth sensor. RealSense D435 is based on active infrared stereo technology which is a combination of various sensing technologies and can function effectively under daylight and lowlight conditions at a reasonable price. To start, data captured from the camera was preprocessed to remove invalid and undesired areas from the depth information. In the next step, it was required to separate the plant from the background (segmentation). In this study, segmentation was done by assuming that plants are green objects in the scene and are in a specific distance range from the camera. Finally, a technique was used for estimating plant height by finding the highest point of plants. The robustness of the proposed method to various changes in the environment was tested on five basil pots in two different environments. Plant height estimation results demonstrated high correlations and low average errors between estimated and actual values.

## Acknowledgments

I would like to thank my advisor, Dr. Kenneth McIsaac, for the opportunity to participate in this degree and for his support, direction, guidance and advice over the past two years.

I would also like to extend my gratitude to Vineland Research and Innovation Centre for their financial support and for the opportunity to do my research at their facilities. Partial funding of this research was provided through the Mitacs organization.

Additionally, I wish to thank Dr. Gideon Avigod and Dr. David Gholami, my supervisors at Vineland. Dr. Gideon Avigod has been an incredible influence on me. I have much to thank him for and most of all I appreciate the opportunities he has provided to me. I would also like to thank Dr. Brian Lynch for his advice and guidance in my last year of research.

I would like to thank all my colleagues at the Vineland Research and Innovation Centre, especially the robotics and automation group: Omar Abdolzaher, Jamie Aiello, Kyung Choi, Kyle Crawford, Dr. Ali Iskurt, Dr. Mohamed Kashkoush, Chris Mohr, Shashank Pandillapally, Jose Rincon, Gurveer Sundhu, and Darren Ward for their friendship, advice and help in the last two years. I would like to especially thank Sydney Stavina and Scott Henderson for helping me with data collection during experiments.

I would also like to thank the greenhouse management team at the Vineland Research and Innovation Centre, especially Cathy Gray and Kevin Meester for their help and advice regarding my experiments.

I would like to thank Freeman Herbs Inc. for letting me visit their place as well as their generous donations of basil for conducting experiments.

Lastly, I would like to thank all my friends and family, especially my husband for their continued support, advice, patience and love through the last two years.

# Table of Contents

Abstract.....	i
Summary for Lay Audience.....	ii
Acknowledgments.....	iii
Table of Contents.....	iv
List of Tables.....	vii
List of Figures.....	viii
Chapter 1.....	1
1 Introduction.....	1
1.1 Importance of Height Measurements of Plants.....	1
1.2 Problem Statement.....	3
1.3 Computer Vision in Agriculture (Challenges and Limitations).....	5
1.4 Objectives.....	8
1.5 Thesis Contributions.....	8
1.6 Thesis Outline.....	9
Chapter 2.....	10
2 Literature Review.....	10
2.1 Plant Phenotyping.....	10
2.2 Non-Destructive Plant Growth Measurement.....	11
2.3 3D Computer Vision.....	15
2.3.1 Triangulation.....	17
2.3.2 Time-of-Flight.....	19
2.3.3 Interferometry.....	20
2.4 3D Imaging Techniques for Plant Growth Monitoring.....	21

2.5 Conclusion .....	33
Chapter 3 .....	35
3 Basil Height Measurement System .....	35
3.1 Algorithm Design.....	36
3.2 Data Acquisition .....	38
3.2.1 Sensor.....	40
3.3 Point cloud Preprocessing.....	43
3.3.1 Depth Cut-Off Filter: .....	44
3.3.2 Select the Region of Interest .....	45
3.3.3 Statistical Outlier Removal Filter .....	46
3.4 Ground Detection.....	48
3.4.1 RANSAC .....	48
3.4.2 Plane Detection using RANSAC .....	49
3.4.3 Plane Equations.....	50
3.5 Camera Misalignment and Slope Correction.....	51
3.5.1 Rotation Matrix from Axis and Angle .....	53
3.6 Background Removal and Plant Segmentation.....	54
3.6.1 HSV Color Space.....	55
3.6.2 RGB to HSV Algorithm.....	57
3.6.3 Color and Depth Segmentation.....	58
3.7 Plant Height Estimation .....	60
4 Experimental Results .....	61
4.1 Preprocessing Results .....	62
4.2 Plane Detection Results .....	64
4.3 Correction Results.....	64

4.4 Image Segmentation Results.....	65
4.5 Plant Height Measurement Results.....	67
5 Conclusion .....	70
5.1 Introduction.....	70
5.2 Summary.....	70
5.3 Conclusions.....	72
5.4 Contributions.....	72
5.5 Discussions & Future Work.....	73
5.6 Abbreviations.....	74
References or Bibliography .....	76
Appendices.....	89
Curriculum Vitae .....	90

## List of Tables

Table 1: Main Specs of Intel RealSense Depth Camera D435 [81] .....	42
---	----



## List of Figures

Figure 1: Manual height measurement in the greenhouses.....	3
Figure 2: Working principle of light curtain arrays(LC) and shoot silhouette extraction [25]. (A) LC are scanning a row of plants (examples of light beams are shown by the red horizontal lines). The blue arrow depicts the movement of LC during the scan. Pot height is 13 cm. (B) Plant Profile of a row of rapeseed plants. The green color shows the segmentation step during which the plant silhouette is separated from the pot silhouette. (C-E) Estimation of maximum height (base to the highest lead tip; depicted by a line) from the silhouette of different sized tomato plants. ....	13
Figure 3: Principles of noncontact 3D shape measurements [35].....	17
Figure 4: Examples of (a) active (light beam) and (b) passive (stereo vision) triangulation [34]. Z is depth, b is basis line, f is focal length and d is the position of the incoming light beam on the detector. ....	18
Figure 5: Basic Principle of an optical TOF ranging system (a) [34] (b) [36] .....	20
Figure 6: Schematic representation of a Michelson Interferometer [34].....	21
Figure 7: LIDAR project a point over the whole image. The detector measures the runtime of the reflection of the laser returning from the object [16]......	22
Figure 8: Laser light section scanners [16].....	23
Figure 9: 3D triangulation laser in [49] .....	24
Figure 10: Example of experimental setup used to implement Structure from Motion in [58]......	26
Figure 11: Stereo vision setup. Stereo vision uses two cameras to measure the same scene. As can be seen on the right, the same object will be in different locations in two	

images. This shift is called disparity and can be used to calculate the distance from camera to this object [16].	27
Figure 12: An example of point cloud generation using Stereo Vision [20]	28
Figure 13: Stereo vision-based plant height measurement system [2].	29
Figure 14: Plant height measurement sensor system [42]. (a) A ground-based platform. Sensors installed on the boom were marked as (1) a Kinect for Windows v2, (2) four DSLR cameras, (3) a LIDAR-Lite v2 sensor, and (4) an ultrasonic sensor. (b) An unmanned aerial platform consisting of an IRIS, quadcopter, a gimbal, and a digital camera.	31
Figure 15: Active infrared stereo vision technology [74].	33
Figure 16: Two different growth stages of basil	35
Figure 17: Height measurement system overview	37
Figure 18: Intel RealSense Depth camera D435 [77]	38
Figure 19: Structure of the plant height measurement in this study	39
Figure 20: (a) An example of RGB image and (b) the colorized depth map, both from RealSense D435.	40
Figure 21: Intel RealSense Depth camera D435 used in this study [80]	41
Figure 22: Active Infrared (IR) Stereo Vision Technology (The depth pixel value is a measurement from the parallel plane of the cameras and not the absolute range as illustrated) [80].	42
Figure 23: An example of depth cut-off filter on an image (noise areas have marked with red)	45
Figure 24: RANSAC separates the given data into inliers and outliers [86].	48

Figure 25: Measuring highest point at two different positions (a) closer to the centre of camera (b) closer to the corner of image. The actual distance of the highest point from camera measured manually and is about 62.9 cm.....	52
Figure 26: (a) The proposed algorithm slightly reduced the depth accuracy when the highest point is in the middle (Figure (25(a))), but it keeps the tolerance in acceptable range. (b) On the other hand, the algorithm improved the depth measurement when pot was located at second position (Figure (25(b)).....	54
Figure 27: Illustration of the HSV color space [98] .....	56
Figure 28: RGB to HSV conversion example (a) RGB image (b) H channel image (c) S channel image (d) V channel image.....	58
Figure 29: Histogram of hue image. Hue values of green color is approximately between 0.25 and 0.45 (marked with red).....	59
Figure 30: Plant height measurement. $h$ : plant height, $z_3$ : z-value(s) for which the rest of the points of the point cloud are below, $z_1$ : the distance of the camera from the ground measured manually, and $z_2$ :the height of the plant pot.....	60
Figure 31: The 3D imaging experiments for sample plants were carried out in two environments: (a) an indoor office with some ambient light coming from the window (b) hangar building under a ceiling light (no window).....	61
Figure 32: An example of point cloud preprocessing: (a) The original image (b) after selecting region of interest (c) after Statistical Outlier Removal filtering.....	63
Figure 33: An example of ground plane detection.....	64
Figure 34: An example of camera misalignment and slope correction for office environment (a) before correction (b) after correction .....	65
Figure 35: Plant identification (a) training (in the office) (b) test (in the hangar).....	66

Figure 36: An example of green plant segmentation based on hue and saturation components .....	66
Figure 37: Demonstration of a maximum point of the canopy (marked with red) .....	67
Figure 38: Comparison between plant height derived from RealSense D435 camera measurements with plant height measured manually (For individual Basils (rows 1 to 5) and for group of Basils (row 6) ) .....	68

## Chapter 1

### 1 Introduction

Diagnosing plant stress in different growth stages seems to be crucial to minimize loss of productivity in the early stages. In conventional greenhouse production, growing statuses are mainly based on human measurement or predetermined environmental parameters instead of considering plants' specific needs at each time. Vision-based systems provide novel solutions in which specific requirements of plants could be determined as well as the overall statuses of plants. This would help to use resources and energy for production more efficiently and in the end improve plant quality, while reducing costs to the customer [1].

#### 1.1 Importance of Height Measurements of Plants

Controlled-environment farming is the combination of science and engineering techniques to apply horticultural technology in controlled environments (greenhouses) in order to enhance crop yields by identification of each plant's particular requirements and more efficient usage of resources and energy for production [1].

There are a variety of factors that can influence crop performance such as soil properties, water availability, pest infestations, climatic variation, and topographic features. Because these factors interact with each other, vary spatially and temporally, and stress crop plants at different times during the growing season, it is difficult to identify the influences of each of these factors on crop growth and yield or to determine how these factors could be managed site-specifically. An important constraint to analyzing factors that limit yield in fields is the lack of proper on-the-go sensing technologies for plant growth [2]. The importance of achieving yield measurement accuracy arises when the goal is to manage fields based on small areas of management in order to optimize inputs such as fertilizers, water, chemicals and output performance as well as reduce environmental pollutions [3].

Crop growth status is one of the highly important parameters in phenotyping. The plant's growth can be extremely affected by environmental conditions. Measuring the plant's growth accurately provides information which can be utilized to speed up crop production [4]. It is also a base for a variety of fields including phenotyping, crop production prediction, fertilizer and water management and other relevant applications [5]. By monitoring the plant's behavior under a certain environmental condition, the results obtained from crop monitoring is useful for comparing crops over time and space and providing more useful data for the greenhouse control system [4].

Plant height is one of the most important components in plant phenotyping since it directly demonstrates plant growth and can be utilized to determine other plant features such as yield and biomass [6]. Plants grow to a specific height in each growing stage. However, the growth rate of plants that are prone to disease and water shortages declines, resulting in less productivity [7].

Plant height is specified as the perpendicular distance between the soil level and the highest point of the main photosynthetic tissues (excluding inflorescences) of a plant. Currently, height is principally measured by human using measuring tape or handheld instruments such as laser and ultrasonic distance meters. Measurement by hand requires considerable effort and time and thus is not suited to large-scale trials. This has been a barrier for many breeding applications as well as genetics [6]. Figure (1) illustrates the traditional height measurement in a greenhouse.



**Figure 1: Manual height measurement in the greenhouses**

In contrast to hand measurement, image-based methods are not only non-damaging but also efficient and can be utilized to obtain a considerable amount of data [8]. Digital imaging of plant growth during its growth stages provides the opportunity for growers to assess the total amount of stress response mechanisms and provides an opportunity to eliminate many of these responses [9].

## 1.2 Problem Statement

The agriculture industry is heavily based on both permanent and seasonal labour. For a long time, traditional ways of plant evaluations were carried out on a small sample of plants from selected product areas which were invasive, laborious, inaccurate, and inefficient [10]. This will be a barrier in applications in which continued monitoring of plants is required.

Automation of greenhouse irrigation is one of the recent fields of research which requires detailed knowledge of the environmental conditions inside the greenhouse, water requirements of the plant, water content of the growing substrate and their effects on plant growth performance. Research has demonstrated that growers can modulate their plant growth by monitoring and controlling substrate moisture content. For example, providing less water may be a way of producing shorter plants [11].

An example of using manual measurements of plant height as an indicator of water stress can be found in [12]. Data from this research demonstrated that corn plant height is a good indicator to describe plant water stress and field measurements of corn plant height can be used to ensure that the irrigation planning model accurately predicts the effects of soil moisture stress on its growth and yield.

The decision on whether to irrigate is usually done automatically, however adding manual irrigation based on the grower's preferences and insight is a common practice. A smart irrigation system that can imitate the decision-making of an expert grower, can plan and schedule irrigation periods at least as well as an experienced grower, which in turn can potentially increase yield for many greenhouses that do not possess such level of human expertise. Implementing 3D vision systems for analysis growth of plants is a very promising way to reduce major production costs through significant savings in human labour. In this framework, much of the traditional labor can be easily replaced by one or two local higher-skill technicians who manage and maintain the whole system. One motivation of our work is to address this problem by proposing a solution to automate plant height measurement in a non-damaging but accurate way. However, some of the outcomes of plant height measurement system might be used later in other applications such as plant traits analysis, automatic harvesting and quality control applications.

Basil plants are grown on a sub-irrigation table (1.6 x 5.2 m). Approximately 820 pots are on the sub-irrigation table. The mean height of the sample plants in these pots are manually checked once a day for the entire growth cycle [11]. Based on observation of manual plant height measurement in some of the greenhouses we observe that traditional height assessment of plants is done in such way that small samples of plants from selected product areas are chosen by researchers or growers to measure the highest point of each pot to the soil surface. Then, the average of these values is used for management decisions, for example, to increase or decrease the amount of water. This practice has to be done during the whole growth cycle and on a regular basis, which is extremely time-consuming due to the number and variety of plants in the greenhouses. On the other hand,



the daily growth of some plants, such as basil, is very small (a few millimeters), and the perception of individuals from the maximum point can lead to wrong decisions, and consequently reduce yield.

To address this situation, a system is required to monitor sample pots on each growing bed. The average of these maximum values from different growing beds is used for management decisions. The proposed crop monitoring system should be able to record data automatically and continuously in a non-invasive way to be used in a commercial greenhouse setting, particularly if it is used for real-time monitoring, decision support systems, and control applications. Furthermore, the system must be robust and integrated into greenhouse crop management operations [4]. Obviously, individual plant height measurement in each plot may need a longer time [6]. To reduce processing time and also to provide more representative crop data, the system should be able to monitor groups of plants rather than an individual plant. It should also provide growers with useful measurements which cannot be easily obtainable by other techniques [13]. In the optimum state, the proposed algorithm to measure a plant's height should be able to apply for other greenhouse plants with small modifications. Ultimately, as much as possible, efforts should be made to avoid major changes to existing greenhouse operations or to impose additional supplies.

### 1.3 Computer Vision in Agriculture (Challenges and Limitations)

Plants are non-static, self-changing systems with complexity in shape and appearance which increase over time. They appear under image resolution and grow in an exponential way over time until growth levels off usually at several  $\text{cm}^2$  size for a single leaf (several times of size change) [14]. For an accurate plant phenotyping, high accurate, high throughput and noninvasive techniques are required. Manual plant trait assessments can impose extra cost and time because it requires properly tuned evaluation scales and adequately trained evaluators. In addition, the subjectivity of raters and fatigue of

experienced staff can lead to a lack of accuracy, repeatability, traceability, and efficiency [7].

Vision-based phenotyping techniques are integrated approaches that greatly extend plant researchers' capability to determine various plant attributes. These techniques can acquire many plant traits precisely, non-invasively and relatively fast that crop researchers cannot obtain. Image-based techniques can be classified into 2D and 3D image-based approaches. While 2D image-based approaches have many advantages in plant phenotyping, there are some constraints in studying 3D plant structures. As an instance, 2D image-based techniques can be used for estimation of curved leaf area or plant volume, but results might be inaccurate. 3D image-based approaches are good candidates to acquire the 3D structure of plants. They do not have the limitations of 2D-image based methods and can properly indicate the plant responses to environmental conditions. As an example, plants can change in shape, structure, color, and pattern under stresses such as drought and extreme temperatures. However, high-throughput phenotyping from a complete 3D model is relatively slow and expensive due to a large number of plants. Based on the context, it may not be essential to reconstruct the entire plant [10]. To estimate organ properties such as accurate leaf size or branching angle, interpretation of 3D data and plant part models are required, but simple measurement of summary traits such as covered volume or plant height can be carried out without 3D reconstruction [14].

In the past decades, many sensing technologies have been developed to acquire 3D information. These sensors are categorized into two types: passive and active. Active sensors are generally sensors with a source of energy that acquire depth data by illuminating the objects they observe and measuring the radiation that is reflected from the target. Common examples of active sensors for depth measurement are laser triangulation and time-of-flight (TOF). On the other hand, stereo vision or structure from motion (SFM) are examples of passive sensors [[15],[16]].

Due to the special circumstances of agricultural environments, not all the available sensing technologies can successfully fulfill the requirements of agricultural applications.

For example, in most agricultural environments, a large number of sensors might be required to cover the whole area in which plants are located. Therefore, to keep the project economical, robust and easy to maintain, machine vision equipment used in such applications should be low-cost technology with low risk of mechanical failure. Furthermore, there are many factors that might influence the design of a vision system for the measurement of plant features including the scale of the plant measurement (i.e. leaf- or canopy-level) and the measurement environment (e.g. a laboratory or under natural daylight) [17].

Several sensor technologies can be used to monitor 3D plant growth. Acquisition of depth data via laser triangulation sensors is very accurate but extra accessories such as a measuring arm or an auxiliary motion system are required. Depth cameras are low-cost tools to acquire depth data. The main drawback of these cameras is their poor performance under strong sunlight. Stereo vision and SFM technologies can provide a low-cost solution for depth measurement as well as a dense point cloud through image processing, but the algorithm is complicated, and the accuracy is limited. It might be necessary to integrate some of the above technologies to improve the performance of the imaging system. Combination of different types of information provides several parameters and thus more possibilities in plant monitoring applications. For example, Zaho [15] in 2018 proposed an integrated system which combines triangulation-based stereo vision for depth information acquisition and grating dispersion for imaging. Therefore, in the time of selecting a 3D sensing technology, the required accuracy, cost, time efficiency, and type of application should be considered [[15],[16]].

The most difficult part of the image analysis of horticultural plants is the separation of the plant from the background. Collection and processing of images with complex structures such as beds or packs of flowering plants are much more challenging and cause many problems. Segmentation of plant leaves from the background is complicated by factors such as the plant type and soil material, the shadows of the plant canopy, the angle of sunlight, the camera angle relative to the canopy and the sun [1].

Evaluations ought to be performed on a case-by-case basis for different growth stages and particularly for various plant types and camera setups. Camera setups can vary broadly depending upon the crop cultivation format. For certain plants, multiple-angle imaging can be commonly used to reduce image occlusions [18].

## 1.4 Objectives

The main objective of this thesis is to propose an accurate height measurement system using low cost sensors which can be used to monitor the growth of crops in greenhouses. The second objective of this thesis is to propose a method in order to improve the system through compensating for slopes in greenhouse beds or any potential camera misalignments which can increase the error in height measurement. The third objective is to propose a general and efficient method for detecting the plant green leaves from the background. Finally, the fourth objective of this thesis to monitor basil plant growth by measuring plant height in different growth stages. To be considered effective for this application, the absolute error of the system must be within  $\pm 5$  mm from a manual measurement.

## 1.5 Thesis Contributions

The main contributions of this thesis are as follows:

- To develop an accurate height measurement of leafy greenhouse plants using commercial sensors.
- To propose methods for ground calibration using RANSAC-based plane detection algorithm and rotation in a three-dimensional Euclidean space by a unit vector (indicating the direction of an axis of rotation), and an angle.

- To develop segmentation techniques in order to distinguish green part areas of basil plant from background to improve the reliability and efficiency of the height measurement.
- To confirm the feasibility of the proposed methods.
- To investigate the possibility of using Intel RealSense active IR stereo cameras as a piece of our vision system to measure the height of plants.

## 1.6 Thesis Outline

The rest of the thesis can be summarized as follows:

- Chapter 2 reviews the background of various methods more specifically, it is focused on the imaging techniques in plant growth analysis and height measurement.
- In Chapter 3 the proposed methods and algorithms are elaborated in detail.
- Chapter 4 presents experimental results of design presented in previous chapter
- Chapter 5 contains a summary of the whole thesis, relevant conclusions, and the outlook to the future work.

## Chapter 2

### 2 Literature Review

This chapter reviews the related technologies and methods implemented in non-destructive plant growth measurement. Section 2.1 discusses the basics of plant phenotyping and its role in developing high yield crops. Section 2.2 describes the concept of non-destructive growth measurement of plants as well as some of the background of different techniques used for plant growth measurement. Section 2.3 describes the basic principles for 3D computer vision. Section 2.4 compares various 3D image acquisition systems for plant phenotyping and plant growth monitoring. Finally, Section 2.5 includes conclusion.

#### 2.1 Plant Phenotyping

Fabio Fiorani and Ulrich Schurr (2013) referred to phenotyping as the series of techniques and protocols used at various organization scales to measure plant parameters such as growth, architecture, and composition with a particular accuracy and precision from organs to canopies. Plant phenotyping is becoming increasingly important due to the requirement to accelerate progress in plant breeding. It combines plant biology sensor technology, and automation engineering to provide a quantitative analysis of plant structure and function related to parameters which leads to better adaptation of plants to organic farming and resource-limited environments [18].

Precise plant phenotyping contributes significantly to analyzing various plant characteristics in different environments. Accurate measurement of phenotypic characteristics during a plant's development stages provides growers with an opportunity to produce high-yield crops with more resistance to disease and higher tolerance to drought and stress. For a long time, traditional ways of plant evaluations were carried out on a small sample of plants from selected product areas which were laborious, inaccurate and had low-throughput and so were recognized as a phenotypic bottleneck in plant

growing programs. Therefore, plant phenotyping has become an expanding field of research in plant breeding in recent years to make the phenotyping an automatic, non-destructive, and high-throughput task [10].

There are various sensor technologies that have been used to improve the procedure of phenotyping in the accuracy and proficiency of phenotyping procedure including visible imaging, hyperspectral and thermal sensing, chlorophyll fluorescence imaging, and 3D imaging systems [19]. Currently, most solutions for plant phenotyping are costly or have been customized to perform specific tasks, thus cannot be practically and generally used in many applications. With the development of low-cost and efficient 3D imaging methods the development of high-throughput plant phenotyping has been facilitated. Apart from reduced price, obtained 3D features of plants can be also used in further applications such as variety selection and the breeding process in modern farming [20].

## 2.2 Non-Destructive Plant Growth Measurement

Among phenotypic parameters of plants, biomass, height, and leaf cover are parameters which indicate the growth stage and physiological status of plants [21] especially for leafy vegetables [5]. Estimation of these parameters can be used as an input in biological modeling and precise agricultural applications. Manual measurement for these parameters as discussed before can be time-consuming and laborious, therefore the study of automatic and non-destructive measurement technology seems to be necessary. Non-destructive growth measurement of plants is the basis for most of applications including phenotyping and breeding, crop production forecast, fertilizer and water management.

Plant height is a fundamental geometric-trait that is not only an indicator of overall plant developmental stage but also a parameter that contributes to the calculation of other advanced parameters such as plant volume and yield. Height information might be specifically utilized in the plant's breeding programs in which large numbers of plots need to be quickly monitored for a subset that are of height suitable for the arranged production and harvesting periods [6]. Additionally, repeated plant height measurement

can be utilized to calculate growth rate and have the ability to describe spatial variation of plant response to inputs and environmental conditions [2] .

In recent decades, many researchers have been working to automate plant height measurement using different sensing methods. Point-based sensors [[22],[23],[24]] are lightweight and affordable tools and thus can be used for low-cost phenotyping applications in fields. Although they could measure plants' height with a good correlation with manual measurements, they do not provide spatial information of plants to measure geometric parameters such as leaf area index and crown volume. Furthermore, the narrow field of view (FOV) of point-based sensors might increase the possibility of excluding the plant highest point and eventually inaccurate height measurement [6].

Light curtain arrays (LC) were introduced to address some of these challenges. They have been used successfully to measure canopy height [[22],[25],[26]]. LC can produce a binary data matrix from which a shoot silhouette is reconstructed. Figure 2 demonstrates the working principle of light curtain arrays (LC) and shoot silhouette extraction. The setup consists of two parallel bars, emit and receive light beams. (Examples are shown by the red horizontal lines). (Figure 2A). The sensor records if the light beams are interrupted by an object or not. By scanning the crop of interest, LC produce a binary data set of the plants' profile (Figure 2B).



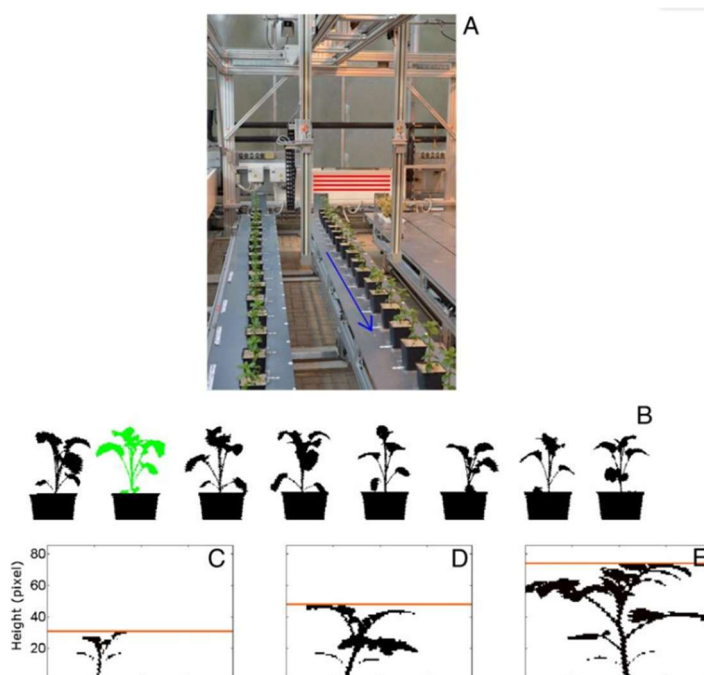


**Figure 2: Working principle of light curtain arrays(LC) and shoot silhouette extraction [25]<sup>1</sup>. (A) LC are scanning a row of plants (examples of light beams are shown by the red horizontal lines). The blue arrow depicts the movement of LC during the scan. Pot height is 13 cm. (B) Plant Profile of a row of rapeseed plants. The green color shows the segmentation step during which the plant silhouette is separated from the pot silhouette. (C-E) Estimation of maximum height (base to the highest lead tip; depicted by a line) from the silhouette of different sized tomato plants.**

The benefit of this method is that height measurement is not affected by the plant distance to the sensor and illumination conditions [25]. However, the resolution of the LC depends on the number of light beams, thus high-resolution light curtains can be costly.

---

<sup>1</sup> Permission is provided through the Creative Common license (CC BY 4), © 2014 by Fanourakis et al.; licensee BioMed Central Ltd.

Furthermore, LC cannot measure 3D structures of the plant and thus complicated geometric features cannot be measured by this method [6].

2D Imaging technique is another way of non-destructive monitoring and analyzing plant growth. The word “2D” refers to the horizontal and vertical dimensions in the image space, as it is a projection of the 3D real world. A 2D camera is a kind of sensor that has the ability to record reflected or emitted light or other electromagnetic radiation from objects by focusing it on a light-sensitive surface [27]. Although automatic measurement of plant growth parameters can be acquired through two-dimensional analysis of a single image, accuracy depends on imaging settings [21].

There are some papers that have focused on the assessment of canopy height using 2D imaging techniques [[28],[29],[30],[31],[32]]. Most of these plant height measurement systems were based on the concept of the visual obstruction method which is used to calculate daily averaged plant heights and their standard deviations and measure the plant height in fields during the whole crop growth period and its interannual changes. In the visual obstruction method, height determination can be affected by the displacement between the referenced scale bar and measured object (i.e. the horizontal distance between the camera and the scale bar is not equal to the distance from the distance between the camera and the object) [29]. In [28], a commercial camera and simple digital image processing techniques such as band selection, filtering and thresholding were used to observe rice crops height changes in a field. The idea was to install a marker bar of known height camera’s field of view and indirectly measure rice crop height by measuring the visible portion of the marker bar. As the rice grows higher, it covers more parts of the marker bar. The results of this paper demonstrated that the direct measurement of the crop height from the longest vertical line is prone to errors. The authors also stated that their measurements may have been inaccurate or unreliable during rainfall events. Mano in [29] proposed a height measurement system using a commercial time-lapse camera using a similar approach to capture seasonal and annual variations in

rice plant height that indicate plant heights at the site scale and improved some of the results.

Constantino *et al.*, 2015 developed a plant height measurement system for greenhouse using current technologies of sensor devices and image analysis. The height was computed by using Euclidean Distance in pixels and then converted to centimeters with 1 cm to 8 pixels ratio. The plant is segmented from the image with HSV segmentation and thresholding. The height was measured by getting its structure using skeletonization and determining the distance. The system showed a percentage error of 17.25% for the height due to the removal of some parts of the plant during the preprocessing stage [7].

The error obtained from the above methods does not fulfill the required accuracy in our study. There may be also restrictions on using some of the above-proposed structures in the greenhouses due to the amount of space they occupy.

Generally, some drawbacks associated with using 2D imaging techniques in plant phenotyping and growth monitoring applications are as follows: Projecting any three-dimensional object onto a two-dimensional plane causes certain distortions that require compensation [29]. The imaging process can be easily affected by changing environmental conditions such as light and rain and thus cause image degradation. In addition, the 2D image is hard to comprehensively describe the plant spatial distributions due to lack of depth information about the scene [10].

With the development of sensors and computer technology, 3D imaging techniques have absorbed researchers' attention as it can provide more accurate measurement and more detailed about spatial morphology of the plants [5]. The rest of this chapter reviews the basic principles of 3D computer vision and previous work on automatic plant height measurement using 3D imaging methods.

## 2.3 3D Computer Vision

Computer vision is referred to as the technology of digitally capturing images of an object using vision-based systems and their numerical processing to extract valuable

information. This process is usually started by connecting a digital camera to the computer and is followed by the development of computer numerical algorithms with the computer based on imaging and kinematic models. Human vision has significantly extended through computer vision in many application fields. Computer vision is superior to human vision where quantitative measurement is desired because of its higher speed and accuracy. Computer vision is closely related to robot vision, machine vision, image processing, image analysis, and pattern recognition [33].

A single image of a scene includes a large amount of information. However, recovery of the geometric information about the scene from a single image is not a simple task since one dimension (depth) is lost in the projection from 3D world to 2D imaging plane. A 3D image is a large collection of distance measurements from a known reference coordinate system to surface points on the objects scene. Depending on the context, a 3D image is also known as range image, depth map, depth image, or 2.5D image. The 3D image provides more information regarding the scene by adding valuable depth information. The 3D imaging methods are crucial for generating robust raw data for appropriate information extraction. The 3D image processing techniques are determined by the quality of generated raw data. Different kinds of spectral waves such as light, ultrasound and microwave can be used to acquire 3D measurement. Optical systems are preferred because of faster 3D acquisition, higher lateral resolution, and safer system setup. Most of the optical systems commonly use three basic principles for depth measurement: triangulation, time-of-flight (TOF), and interferometry [34]. Figure 3 demonstrates the family tree for contactless 3D shape measurement.

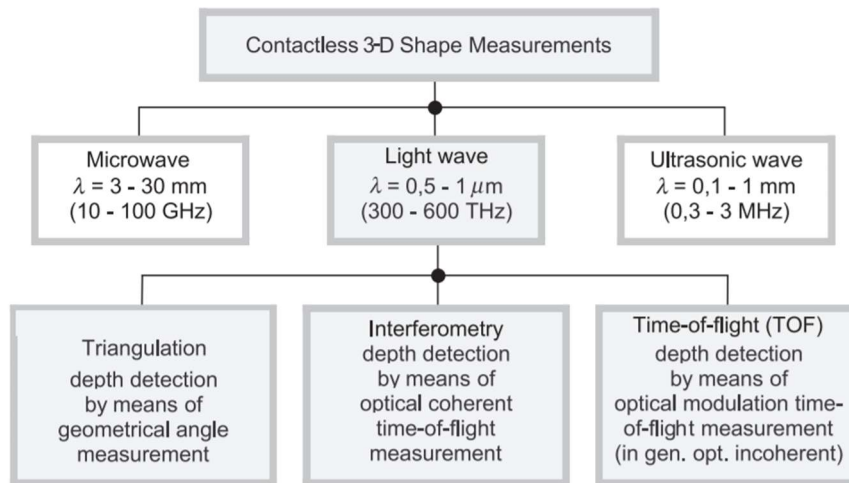


**Figure 3: Principles of noncontact 3D shape measurements [35]<sup>2</sup>**

### 2.3.1 Triangulation

Triangulation approach is in the shape of stereo vision and depth-of-focus system and is similar to human depth perception. Triangulation is a geometrical methodology in which the object is one point of a triangle and the two other points are known parts of the measurement system. The distance of the object can be determined by measuring the triangle's angles or the triangulation base. Triangulation can be divided into active and passive groups. Digital photogrammetry methods such as stereo vision and structure from motion are considered as passive triangulation for the generation of a 3D image while structured light is categorized as active triangulation. Stereovision is one of the most popular examples of passive triangulation methods which uses at least two image sensors to observe the scene from different angles. Using passive triangulation techniques, a scene with high contrast is required because it is necessary that each point that is part of measurement can be clearly found by both viewing positions [36]. Figure 4 illustrates the examples of active and passive triangulation techniques.

---

<sup>2</sup> Reproduced with permission, © 2000 by Academic Press

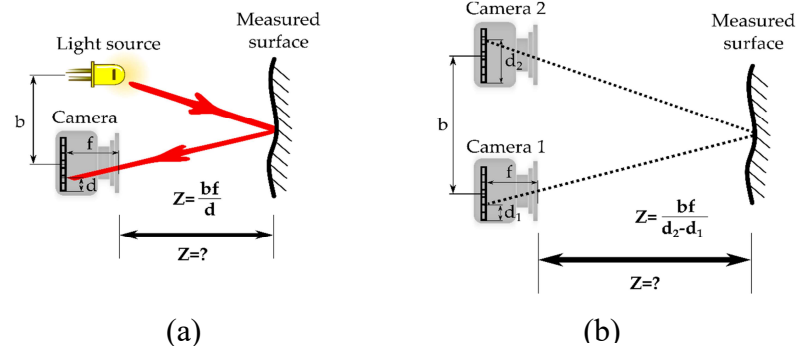


**Figure 4: Examples of (a) active (light beam) and (b) passive (stereo vision) triangulation [34]<sup>3</sup>.  $Z$  is depth,  $b$  is basis line,  $f$  is focal length and  $d$  is the position of the incoming light beam on the detector.**

Active triangulation utilizes a light source to illuminate the scene which is observed by a position sensitive detector. Instead of directly measuring angles, active triangulation relies on the similarity of triangles (the target triangle and the image triangle) which is adequately determined by the optical axis of the imaging device, the focal length  $f$  of the system and the position of the point projection  $d$  on the detector. To obtain the distance  $Z$  of the target, displacement  $b$  of the light source from the imaging device must be known. In the simplest case, the projected light is a point. Available triangulation systems can be used for mm-range (depth of focus) to 100-kilometer range (photogrammetry) measurements.

One of the main disadvantages of triangulation systems is their large size. The reason is that to obtain a good resolution, they require a large triangulation base. The larger this triangulation base, the more they are restricted by shadowing effects. Furthermore, as 3D triangulation systems require fast LCD projectors (in active systems) and large computational power, their price is relatively high [36].

---

<sup>3</sup> Permission is provided through the Creative Common license (CC BY). © 2016 by Vázquez-Arellano et al; licensee MDPI, Basel, Switzerland.

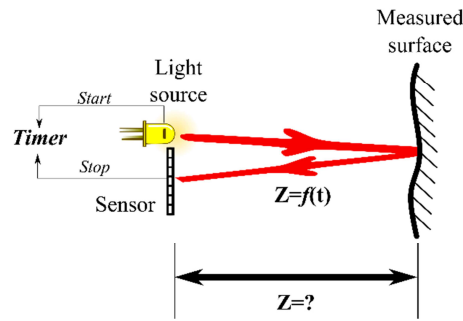
### 2.3.2 Time-of-Flight

Time-of-flight (TOF) is defined as the time that the light needs to travel from the measurement system to the object and back again and corresponds directly to the distance  $R$ .

$$TOF = \frac{2R}{c} \quad (1)$$

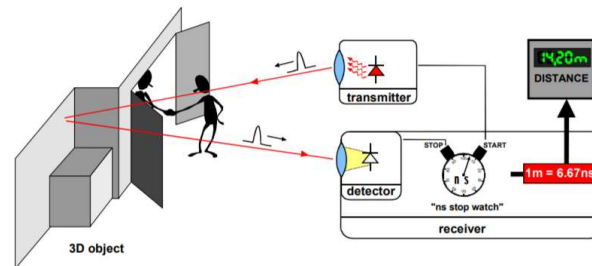
In this equation,  $c$  is the light velocity and is equal to  $3 \times 10^8$  m/s. The method is best for measurements ranges from some centimeters to several hundreds of meters where relative accuracies of 0.1 percent are required. Therefore, millimeter range standard deviations can be realistically obtained at absolute distances of some meters with a time-resolution of 6.6 picoseconds.

Figure 5 shows the basic Time-Of-Flight principle. The basic principle of time of flight systems can be summarized as follows: A light source sends out a light pulse and turns on a very accurate stopwatch. The light pulse goes to the object and back. When the reflected light pulse is received by the detector, the stopwatch will be stopped and the time of flight of the light pulse is determined. The light pulse travels the distance two times (forth and back), thus every 6.67 ns corresponds to a one-meter distance. A fundamental feature of this configuration is that the sender and receiver are synchronous. Since directions of illumination and observation are collinear, the TOF ranging technique does not generate incomplete range data (no shadow effects). This is a significant advantage of a TOF ranging system over a triangulation based system. Obviously, a basic problem of TOF systems is that to establish 1cm TOF- resolution, higher accuracy is required (6.6ps for 1mm) [36]. In order to realize such a system with discrete components, as is done in today's TOF rangefinders, it is necessary that each component in the signal chain have a very high system bandwidth [37].



Distance  $Z$  is dependent on the time  $t$  that takes a light pulse to travel forth and back

(a)



Every 6.67 ns corresponds to a one-meter distance

(b)

**Figure 5: Basic Principle of an optical TOF ranging system (a) [34]<sup>3</sup> (b) [36]<sup>4</sup>**

### 2.3.3 Interferometry

Optical Interferometry is one of the most precise basic principles that can provide nanometer range accuracies. In Michelson interferometry, the simplest case of interferometry, a coherent light beam is split into two similar beams by a splitter which is a partially reflecting mirror. one of these beams travels towards the reference mirror while the other is projected towards a target. Both beams are then reflected to the splitter and projected towards a detector which creates a phase difference between the beams to

<sup>4</sup> Reproduced with permission from Robert Lange (2006).



calculate the relative depth (Figure 6). Depth  $Z$  is straightly relative to the number of fringes  $n$  and wavelength of the light source  $\lambda$  [34]. More information regarding this principle can be found in [[36],[38]]

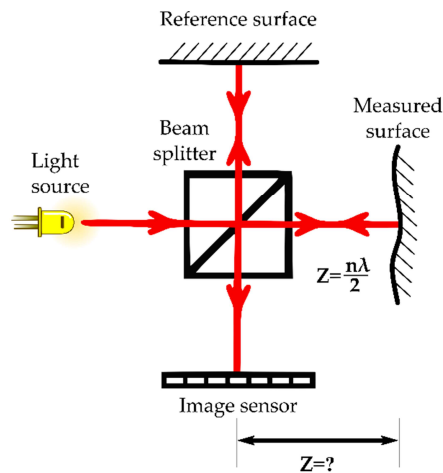


**Figure 6: Schematic representation of a Michelson Interferometer [34]<sup>3</sup>**

## 2.4 3D Imaging Techniques for Plant Growth Monitoring

Due to the complexity of agricultural environments, measuring vegetation requires advanced image analysis. According to Vázquez-Arellano et. al (2016), there has been a fast growth in the number of scientific papers related to agricultural 3D vision systems in the last decade. In that review, some motivations for this tendency have been mentioned, including the steady increase in computer processing power, the reduction in cost and size of electronics, the increase in the efficiency of solid-state lighting, the unique non-contact and non-destructive properties of machine vision technology and the demand for higher knowledge and care for the individual crops. The focus of some existing implementations that use 3D vision systems for agricultural applications lays on vehicle navigation, and crop and animal husbandry [34].

Various 3D imaging techniques are available in the market. Laser sensor techniques provide accurate measurement of 3D plant structures. As an example, Chaudhury *et al.*

[39] proposed a fully automated system with the capability of analyzing plant growth throughout its life cycle using a 3D laser scanner.

LIDAR is an active remote sensor that is used to measure the distance to a desired object based on the TOF principle [40]. It has become popular in precision agriculture, forestry, and plant phenotyping applications [41]. As it can be seen in (Figure 7), it sends out a small dot onto the targets using a combination of a detector and a laser which is moved at high speed over the whole scene while a detector samples it. The detector measures the runtime between the emission and return of laser from the target [16]. The movement is often obtained by using one or more rotating mirrors.

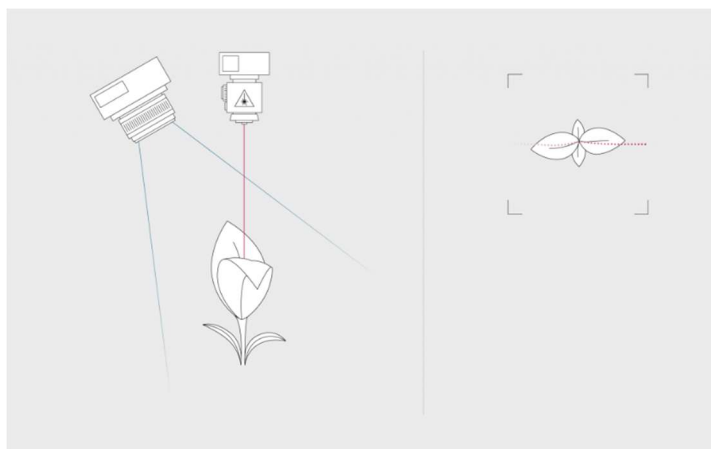


**Figure 7: LIDAR project a point over the whole image. The detector measures the runtime of the reflection of the laser returning from the object [16]<sup>5</sup>.**

Obtained 3D data from LIDAR techniques have the potential to provide high-resolution topographic maps and highly accurate measurements of crop height, cover, and canopy structures [[42],[43],[44],[40],[45],[46],[41],[47]]. LIDAR has been used in applications from distance ranges of thousands of kilometres to centimetres, which shows the ability

---

<sup>5</sup> Reproduced with permission from PHENOSPEX

of these sensors [48]. Friedli *et al* [41] proposed a terrestrial laser scanner for measuring canopy height growth of different crops under field conditions. High-resolution portable scanning lidars have been used to extract precise plant height in greenhouses [47]. LIDAR is a very fast technology, light-independent and provides high scanning range. However, as Lidar is point-based technology, it provides a narrow field of view and therefore the highest point of plants might be frequently lost [16]. In addition, wind and movement during data capturing could make plants move, leading to inaccuracy in measurements [40]. Although many studies show that LIDAR can be a useful tool in plant features analysis, it still needs to be improved in terms of throughput, cost, and complexity [10].

3D triangulation laser scanner is another sensing technology that is used to measure 3D distributions of plants [49]. Laser light section scanners are similar to LIDAR in terms of projecting a laser on the object but different than LIDAR as it projects a line instead of point. Unlike LIDAR, laser light scanners compute the distance of the objects to the camera by measuring the shift of the projected light and not the runtime of it (Figure 8). The laser line is shifted by any object in the image in function of the distance towards the sensor. These systems are robust as they do not have moving parts and can have high precision and high resolution.

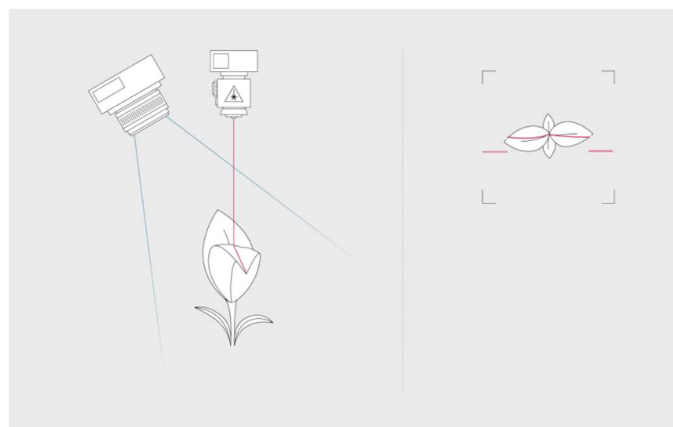


**Figure 8: Laser light section scanners [16]<sup>5</sup>**

A triangulation laser was used in a lysimetric platform to assess canopy attributes of plants [50]. Furthermore, a 3D triangulation laser scanner was used to measure daily changes in plant growth of rapeseed plants with high precision in challenging environments [49] (Figure 9). The results from these studies show that laser triangulation is a suitable methodology for high-precision plant phenotyping. However, the price of device is relatively high [10]. Furthermore, the scanner must be calibrated to a certain range, resulting in less flexibility. Similar to LIDAR, as it is a scanner, the system requires to constantly move over plants or plants needs to be moved below the scanner which takes some time. Movement of plants due to wind or other reasons might affect the quality of the 3D point cloud [16].

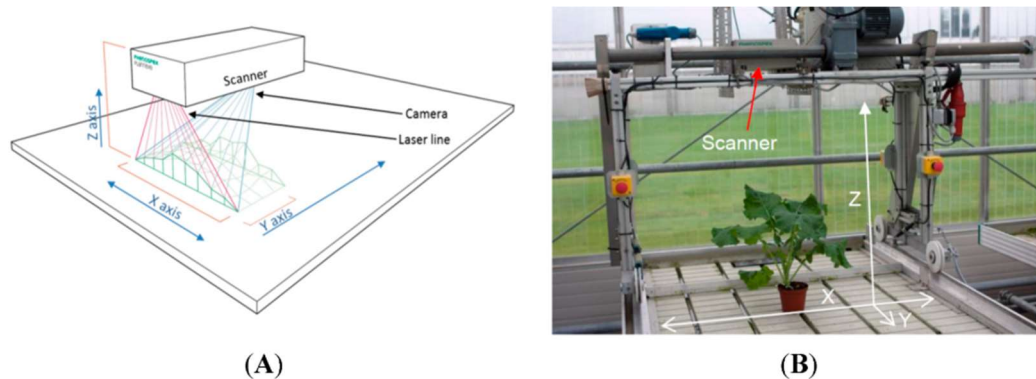


**Figure 9: 3D triangulation laser in [49]<sup>6</sup>**

The structured light method is based on illuminating special IR patterns or multiple lines to the object rather than a line (Laser) or one point (lidar). This technique is widely utilized in commercial applications, but less in plant study [[51],[52],[53]]. One of the main disadvantages of these sensors is that their internal light patterns can be easily affected in the greenhouses by daylight or existing lighting systems [16].

---

<sup>6</sup> Permission is provided through the Creative Common license (CC BY), © 2015 by Kjaer and Ottosen; licensee MDPI, Basel, Switzerland.

Time-of-flight (ToF) sensors are another device used to acquire 3D information for 3D plant analysis [[54],[55],[56]]. It has been shown [54] that the combination of dense color data and sparse depth obtained from ToF camera can provide a fair 3D approximation for high throughput and automatic plant measurements in robotic applications. ToF cameras provide high frame rate and accurate depth measurements under suitable conditions [55], but they might not be suitable candidates to use under strong sunlight because they also use infrared emitters to measure the time it takes for the signal to be reflected. Furthermore, they provide poor resolution relying on the object reflecting surface and color [16]. Busemeyer *et al.* [22] used 3D ToF cameras for the canopy height measurements of the small grain cereals in field from top view. They got the mean relative error (MRE) ranged from 4.3% to 6.5%. In very recent paper, Guan *et al* [57] developed a low-cost, novel, and efficient imaging system consisting of a RGB camera and a photonic mixer detector (PMD) and demonstrated the usability of it for plant height measurement from top and side view. They yielded a determination coefficient ( $R^2$ ) of 0.9890 and 0.9936 for the estimation of soybean height from the side and top view respectively.

Structure from Motion (SFM) is another low-cost technique that can be used to obtain plant 3D information using 2D images or videos captured by a single camera acquiring images while moving along the row [[8],[58],[59]]. The point cloud obtained by this method is high resolution, but the algorithm itself is complicated. However, using SFM to obtain the crop row 3D structure is simpler than using stereovision with multiple cameras. The reason is that the camera intrinsic parameters are automatically estimated during the reconstruction process and thus no initial calibration is required. An automatic plant growth measurement system has been developed to non-invasively and continuously measure Boston lettuces weight and growth features cultivated in the plant factory [8]. Jay *et al.* [58] proposed a method to retrieve row structure and structural components such as plant height and leaf area using SFM to estimate plant height and leaf area. Plant and background were segmented using both color and height information to deal with low-contrasted areas. They also could get the best overall accuracy in cases

that the contrast is high because using height information. The efficiency of the proposed approach was assessed with two data sets collected under outdoor conditions. Robustness of the model was evaluated against different plant structures, sensors, imaging techniques and lighting conditions. The crop row 3D models were accurate and led to satisfactory height estimation results. However, there were some issues such as occlusion and plant changing position from one image to the other because of the wind.

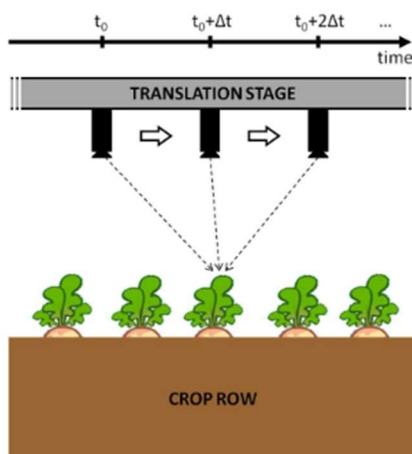


**Figure 10: Example of experimental setup used to implement Structure from Motion in [58]<sup>7</sup>.**

The most common imaging techniques used for plant growth monitoring in indoor and outdoor conditions is stereo vision [[2],[60],[61],[62], [59],[63],[20][15]]. Stereo vision uses two cameras mounted next to each other to view the same scene. As shown in Figure 11 the same object is at different positions on the two images since the perspective of the cameras is slightly different (1 and 2). The distance from the camera to that object can be

---

<sup>7</sup> "Reproduced from Computers and Electronics in Agriculture, Vol 110, Sylvain Jay, Gilles Rabatel, Xavier Hadoux, Daniel Moura, Nathalie Gorretta, "In-field crop row phenotyping from 3D modeling performed using Structure from Motion" / Chapter 2, Page 2, Copyright (2014), with permission from Elsevier."

calculated based on the “shift” of the object from left to right from one image to the other which is called disparity. objects closer to the stereo setup have a bigger disparity than further ones [16].

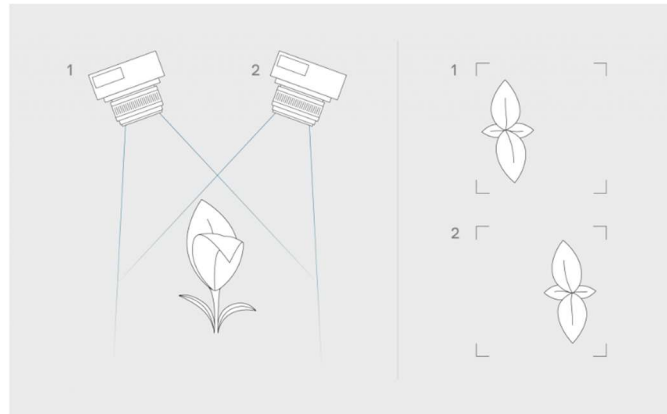


**Figure 11: Stereo vision setup. Stereo vision uses two cameras to measure the same scene. As can be seen on the right, the same object will be in different locations in two images. This shift is called disparity and can be used to calculate the distance from camera to this object [16]<sup>5</sup>**

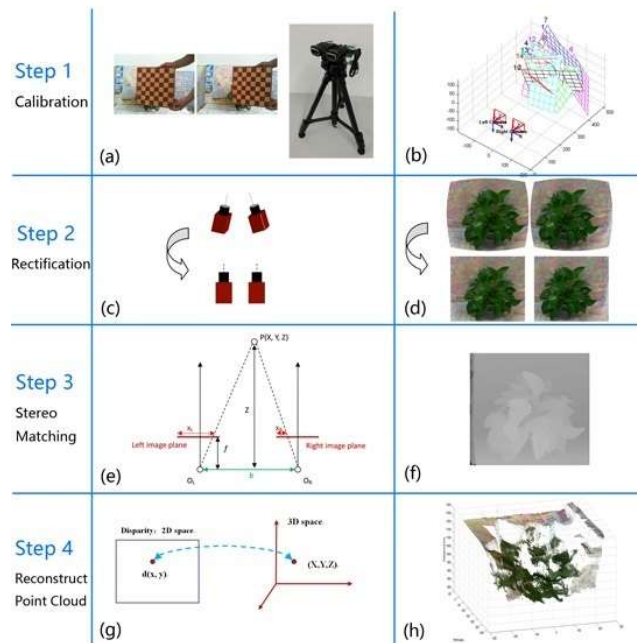


**Figure 12: An example of point cloud generation using Stereo Vision [20]<sup>8</sup>**

Passive Stereo vision offers the depth information by searching the correspondence between the images taken by the cameras and then doing triangulation [10]. Stereovision methods can be implemented using inexpensive commercial sensors and if a proper RGB camera is used, stereovision can provide both color and the 3D structure estimation [5]. Stereo vision can be used to monitor plant parameters including height, leaf shape and leaf area for young plants and overall canopy dimensions for larger crops [17]. Stereo vision systems have main drawbacks. The depth resolution in depth is relying on the structure of the object, local contrast and the angle of sensors to each other [16]. They are susceptible to light changes of the scene and they require a powerful computational system to perform stereo-matching algorithms. These limitations arise in outdoor environmental conditions because image segmentation becomes also a challenge [48].

<sup>8</sup> Permission is provided through the Creative Common license (CC BY), © 2017 by Li et al. Licensee MDPI, Basel, Switzerland.



Reflection of sunlight creates bright white color regions on the surfaces of large and smooth leaves called *highlight regions*. Highlighted regions lose texture details, which is a barrier for many stereo matching algorithms. The recent study [20] established an inexpensive and portable stereo vision system in generating dense and accurate 3D imaging of plants to work under indoor lab, open field with grass, and multi-span glass greenhouse environment. They proposed a method for recovering 3D surfaces of highlighted leaf regions.

A stereo vision-based plant height measurement system has been developed to measure corn plant height [2]. A single camera was used on an imaging platform. The movement of the camera was precisely controlled using a microcontroller. Plant height was estimated by triangulation using pixel disparity between two images were taken of the top view of the plant from a standard stereo configuration. The developed stereo vision system estimated maximum plant height with an RMSE of 2.55 cm.

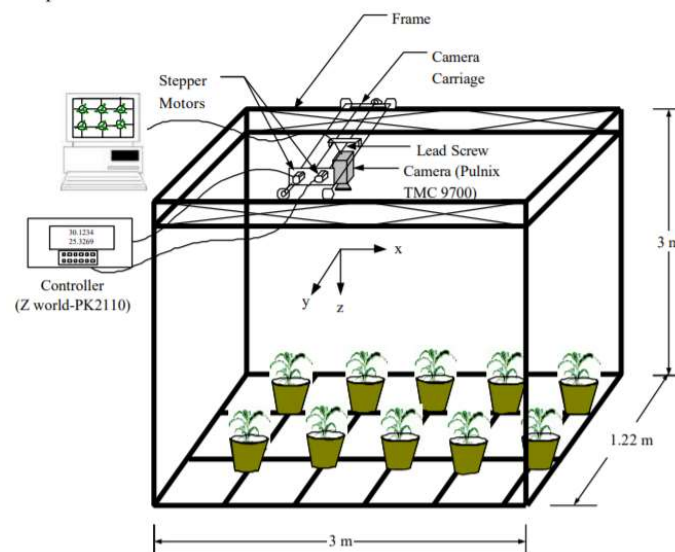


**Figure 13: Stereo vision-based plant height measurement system [2]<sup>9</sup>.**

<sup>9</sup> Reproduced with permission, Shrestha et al. (2002)

Recently, commercial 3D imaging sensors absorbed the attention of researchers in the field of phenotyping because of high efficiency and low price. Light-field camera, also called to as a plenoptic camera delivers two images of the object: a focus image, similar to that captured by a typical 2D camera, and a depth image [64]. To create a 3D topological map of the imaged object, these images are combined. Apelt *et al* in [64] introduced a light-field camera system for accurate measurement of morphological and growth-related features in plants. The results from another paper [65] also demonstrated that light field camera (Lytro LF) can be used as a suitable device for environmental monitoring applications, but its scope is restricted to close-range applications. However, to be used in a wider range of applications, the price of light field cameras still has to be reduced.

Customer grade RGB-D cameras are inexpensive cameras with high frame rate and therefore have been widely used in robotics and vision applications. RGBD cameras acquire color images with depth information together at the same time. Kinect (v1), and Kinect (v2) are the most common RGBD cameras release by Microsoft. The first generation of Kinect is based on structured light to acquire 3D information and it has been utilized to measure growth measurement in some literature [[66],[67]]. The second version of Kinect is based on ToF sensing technology. Technically, Kinect (v2) demonstrated a higher resolution and better accuracy rather than Kinect (v1). Furthermore, it has shown promising results in measuring plant growth in outdoor applications [[6] ,[42],[68]]. However, Microsoft has made the decision to stop manufacturing its Kinect Depth Sensor [69].

Yu Jiang *et al.* [6] showed that the Kinect-v2 camera could acquire valid depth images of cotton plants under field conditions when a shaded environment was provided. The performance of for sensing technologies including an ultrasonic sensor, a LiDAR sensor, a Kinect v2 camera, and an imaging array of four high-resolution cameras have been assessed on a ground vehicle platform [42] (Figure 14(a)) and compared with the performance of a digital camera on a remotely controlled vehicle (Figure 14(b)). The comparison results demonstrated that the heights measured on the ground vehicle

platform had a higher correlation ( $r=0.90$ ) with the manual measurements than those heights measured by remote imaging ( $r=0.73$ ).



(a)

(b)

**Figure 14: Plant height measurement sensor system [42]<sup>10</sup>. (a) A ground-based platform. Sensors installed on the boom were marked as (1) a Kinect for Windows v2, (2) four DSLR cameras, (3) a LIDAR-Lite v2 sensor, and (4) an ultrasonic sensor. (b) An unmanned aerial platform consisting of an IRIS, quadcopter, a gimbal, and a digital camera.**

Kinect v2 also used to measure growth analysis of potted plants. Hu *et al* in [5] proposed an automatic system for non-destructive growth measurement of potted leafy vegetables, based on Kinect v2 sensor. Multi-view point clouds of the measured plant were acquired with a turntable. They could achieve very good accuracy, but their method was comparatively slow.

Intel RealSense sensors are other examples of RGBD cameras. In [70], the automated use of the Intel RealSense SR300 was explored to perform phenotyping experiments on basil

---

<sup>10</sup> Permission is provided through the Creative Common license (CC BY 4), © 2018 by Wang et al.

in a hydroponic system with controlled environment. The system showed a mean absolute error value of 8.47mm for the height. However, SR300 working principle on which depth images capture is based on structured light and therefore this camera functions best indoors or in a controlled lighting situation [71].

Newer types of cameras combine different technologies to deliver better performance and a wider range of application with the best price. As an example, Intel RealSense D400 cameras combine active IR pattern emitters with IR stereo cameras and as a result, these depth cameras can work well under low light conditions [72]. Intel's RealSense sensor is a well-known active and optionally passive stereo sensor. Active stereo resembles passive stereo as they both are matching features from one camera to another. However, passive stereo is not able to find features (textures) in uniformly colored surfaces to match. Active stereo sends out a random pattern onto the scene by which even texture less surfaces can be matched between the two views. Furthermore, active stereo cameras have the potential to switch back to passive stereo in cases where the pattern cannot be projected successfully, for example in outdoor lighting or over large distances. All stereo-based solutions (including structured light) typically provide very good x/y resolution. Therefore, they can be used in applications that tiny objects need to be identified, but their problem is shadowing effects. At large distances both cameras see almost similar but close up the two cameras can observe very different segments of objects. Because depth maps are often computed from the point of view of one camera, an object casts a shadow on itself where no depth data is available. Active stereo sensors are one of the most hardware component intensive solution because they include two cameras, one projector and, other accessories for real-time processing [73].

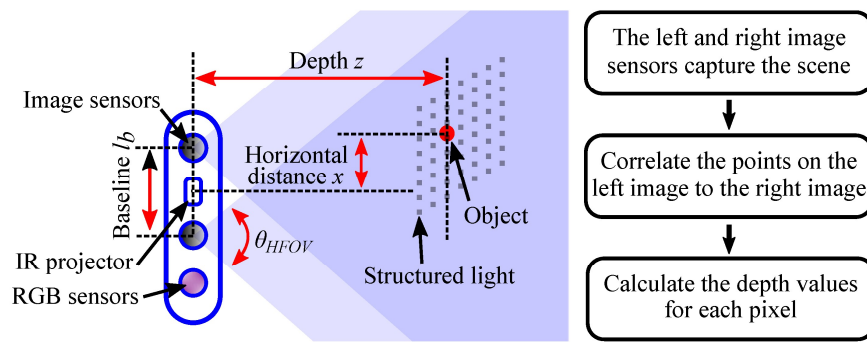


**Figure 15: Active infrared stereo vision technology [74]<sup>11</sup>**

There are not many existing implementations that use RealSense cameras for plant growth monitoring. However, in a recent paper, the performance of modern RGB-D camera including Intel D435 was compared for plant feature measurement in different distances and light conditions. The results from this study demonstrated that modern RGB-D camera, particularly, the Intel D435 camera, provides an applicable device for close range phenotyping applications in outdoor experiments [75].

## 2.5 Conclusion

Many previous efforts of computer vision have been successfully used to determine different plants or leaf growth status with different devices. Based on the literature review, the following conclusions were made. Monitoring and sampling from the crop as a canopy are more favorable than individual plants [4]. The authors indicated the importance of height information in plant segmentation when there is low contrast between plant and background. In these studies, most of the presented imaging techniques used to derive the morphological traits of plants have been designed for specific tasks, they are relatively expensive or required a high level of methodological effort during outdoor measurements and, therefore, resulted in the reduced capability of

---

<sup>11</sup> Permission is provided through the Creative Common license (CC BY 4), © 2018 by Liu et al. Licensee MDPI, Basel, Switzerland.

using in all applications. Kinect v2 demonstrated good results in measuring plant growth in outdoor environments while it is affordable. However, it is not produced anymore. A recent paper suggested D435 as a reliable tool for plant growth analysis in outdoor environments. Considering the challenges and limitations associated with the application of plant analysis in greenhouse environments (i.e. the need for a large number of sensors because of the greenhouse building layouts, the need for high resolution, and the complexity of the greenhouse environment and the plant itself), the RealSense D435 camera was selected to accurately measure canopy height measurement of basil plants in greenhouses as it benefits of both active and passive sensors. In the following chapters, more details are provided on the sensor characteristics and implementation of the height measurement system.

## Chapter 3

### 3 Basil Height Measurement System

Basil plants are one of the plants for which poor environmental conditions can affect their yield. For example, they need consistent soil moisture to yield well [76]. One of the major greenhouses in Ontario was visited to identify important factors in the design of the basil plant height measurement system, which is the subject of this research. At this greenhouse, the basil seeds are planted in 4-inch size pots and placed by the robots in their growing beds. After several weeks, they are rearranged to create more space for growth, but after a certain stage of growth plants starts to overlap each other and since then they cannot be distinguished individually by camera or even human eye. The basil plants will be sent to the packaging area when they reach a certain height. Figure (16) demonstrates images from different growth stages for basil plants.



**Figure 16: Two different growth stages of basil**

As it can be observed in Figure 16(b) the individual plants are not recognizable any longer and height of plants is requiring collective measurement. There are certain challenges associated with this work including vastly different environmental conditions

(e.g., light, humidity, temperature), the complexity of the background, and the slope of beds.

### 3.1 Algorithm Design

To achieve the accurate height of plants from data provided by the Intel RealSense D435 camera, the following algorithm was developed using IntelRealSense library, and MATLAB Computer Vision System Toolbox. The framework of the algorithm is shown in the flowchart in Figure 17 and stated as follows:

Step 1: Data acquisition. The algorithm starts with data acquisition in order to acquire a depth image which contains 3D spatial information with corresponding 2D color information through the sensor.

Step 2: Preprocessing. It is needed to remove noise and undesired pixels from 3D point clouds.

Step 3: Ground detection. In this study, the ground plane is the plane where plants stand on. This algorithm receives processed point cloud as input and fits a plane equation using MSAC and returns inliers and outliers indices.

Step 4: Camera misalignment or/and ground slope correction. Due to the accuracy requirement of the project, the fitted plane is needed to be parallel to xy-plane. This is done by rotating of the point cloud using Euler formulation

Step 5: Background removal and plant segmentation. All the points below a certain threshold where the plant is starting to grow are removed from the point cloud. The threshold is set according to the edge of the pot and can vary based on pot size. Green pixels from the scene are identified in the HSV color space and the rest of the pixels were removed from the point cloud.



Step 6: Height measurement. The remaining points which belong to plants are considered to calculate height.

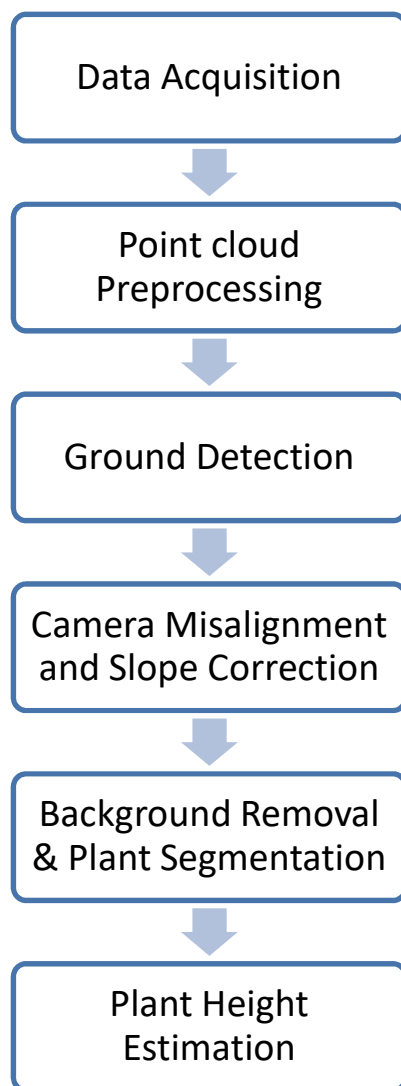


**Figure 17: Height measurement system overview**

## 3.2 Data Acquisition

This stage includes both hardware and software systems for data acquiring. In this study, a calibrated RealSense D435 sensor (Figure 18) was used to capture images of basil plants at the site.



**Figure 18: Intel RealSense Depth camera D435 [77]<sup>12</sup>**

The photo resolution was set to the resolution of 640x480 pixels. The camera was mounted on a handmade metal structure at a height of 80 cm length from the ground to the center of the camera lens) and levelled approximately on the horizontal plane. The camera was pointed downward to the scene. Figure 19 demonstrates the structure of the plant height measurement developed in this study.

---

<sup>12</sup> Reproduced with permission, © Tsukasa Sugiura

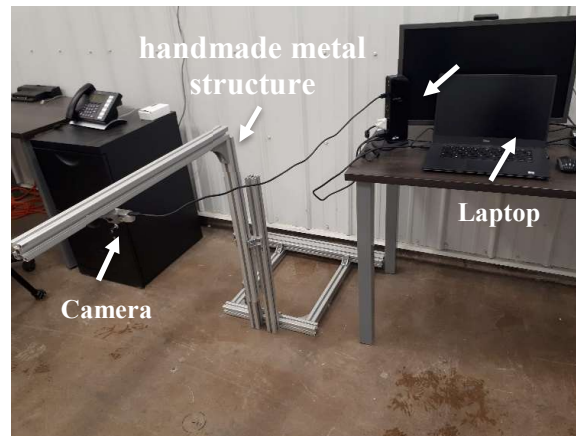
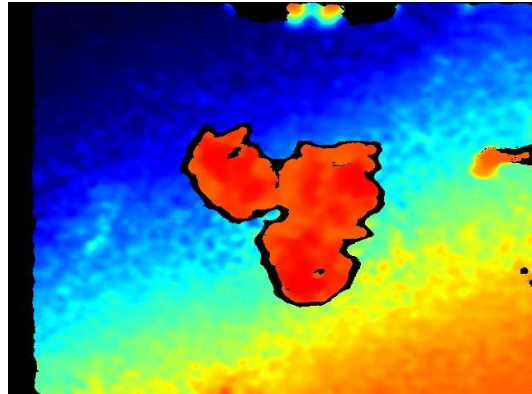


**Figure 19: Structure of the plant height measurement in this study**

In this work, IntelRealSense library which enables communication with RGB and depth cameras of Intel RealSense is used for data acquiring. Different wrappers are available for this library including Python, C#/.NET, Node.js API as well as integration with the following technologies: ROS, ROS2, LabVIEW, OpenCV, PCL, Unity, MATLAB, OpenNI, and UnrealEngine4 [78], For the rest of the project, MATLAB computer vision toolbox [79] is used for processing depth image. Figure 20(b) shows the colorized depth map which was extracted for the image shown in Figure 20(a). As can be seen from the figures, the depth sensor provides a wider field of view in comparison with the RGB sensor.



(a)



(b)

**Figure 20: (a) An example of RGB image and (b) the colorized depth map, both from RealSense D435.**

RGBD images and colored point clouds can be created through color registration. Color registration is the act of assigning colors to their corresponding pixels in depth images. It can make the application simpler due to the unified data structure while simultaneously decrease the cost of memory storage [27]. In Intel RealSense camera the registration function is provided in RealSense SDK by the manufacturer.

### 3.2.1 Sensor

The RealSense D400 series cameras, developed by Intel, uses stereo vision to calculate depth and consists of two main parts, Vision Processor D4, and Depth Module. The

depth module includes left and right imagers, an infrared projector, and an RGB color sensor. The data from the RGB color sensor is sent to the Vision Processor through the color Image Signal Processor (ISP).

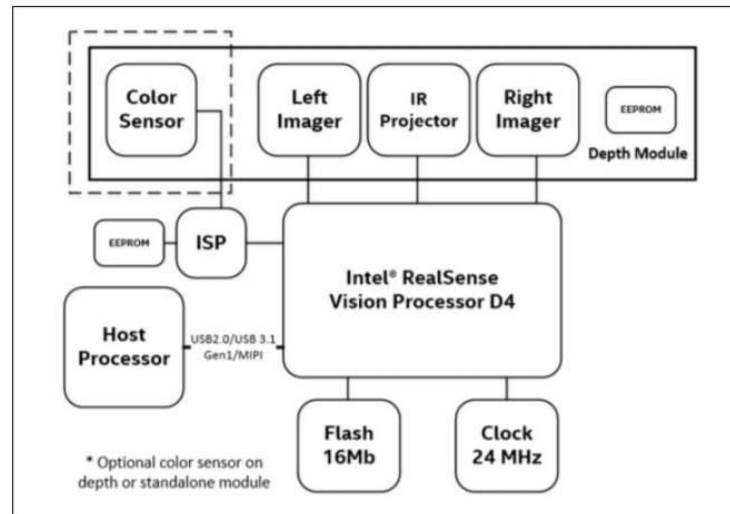


**Figure 21: Intel RealSense Depth camera D435 used in this study [80]<sup>13</sup>**

The infrared emitter projects an invisible static IR pattern to enhance the accuracy of depth in low texture scenes. The obtained data from left and right depth sensors are processed in the vision processor to calculate depth values per pixel in the image by corresponding points on the left image to the right image and via shift between a point on the left image and the right image [80].

---

<sup>13</sup> Reproduced with permission, © 2019 Intel Corporation

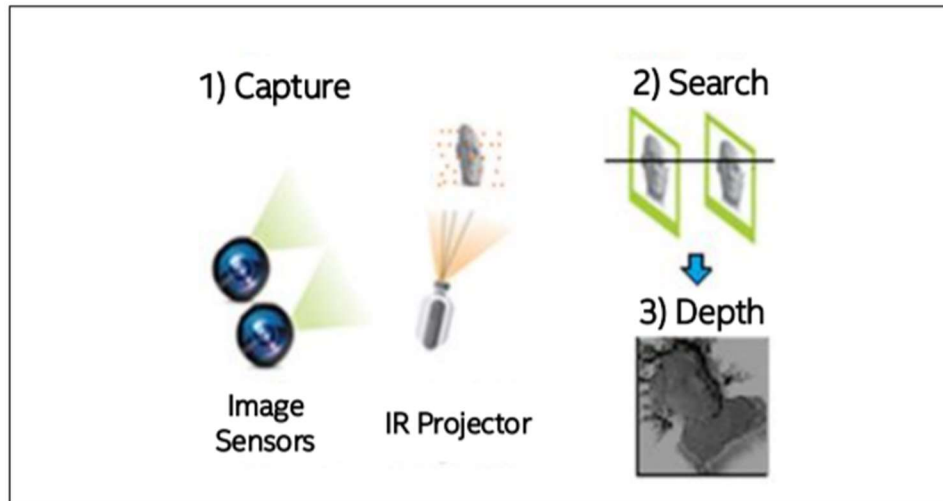


**Figure 22: Active Infrared (IR) Stereo Vision Technology (The depth pixel value is a measurement from the parallel plane of the cameras and not the absolute range as illustrated) [80]<sup>13</sup>**

The specifications of RealSense d435 sensor are listed in Table 1.

**Table 1: Main Specs of Intel RealSense Depth Camera D435 [81]<sup>13</sup>**

Environment	Indoor and outdoor
Depth Technology	Active IR stereo
Image Sensor Technology	Global shutter: 3 um x 3 um pixel size
Main Intel® RealSense™ Products	Intel® RealSense™ vision processor D4 Intel® RealSense™ module D430
Depth Field of View (FOV)—(Horizontal × Vertical) for HD 16:9	85.2° x 58° (+/- 3°)

Depth Stream Output Resolution	Up to 1280 x 720
Depth Stream Output Frame Rate	Up to 90 fps
Minimum Depth Distance (Min-Z)	0.11 m
Maximum Range	Approximately 10 meters  (Accuracy varies depending on calibration, scene, and lighting conditions)
RGB Sensor Resolution & Frame Rate	1920 x 1080 at 30 fps
RGB Sensor FOV (Horizontal x Vertical)	69.4° x 42.5° (+/- 3°)
Camera Dimension (Length x Depth x Height)	90 mm x 25 mm x 25 mm
Connector	USB Type-C*
Mounting Mechanism	One 1/4-20 UNC thread mounting point  Two M3 thread mounting points

### 3.3 Point cloud Preprocessing

Data captured by optical sensors usually include noise, which needs to be filtered and corrected. Failure to remove this noise can lead to unexpected results [27]. Through preprocessing, an effort is made to remove useless data from depth image including sparse noise, the sensor bad points. The undesired regions (regions that contain objects that are not part of measurement) can be also removed from the point cloud. In this study,

the following filters are applied on the point cloud obtained from Intel RealSense depth sensor.

### 3.3.1 Depth Cut-Off Filter:

Since bad points from the sensor usually have a distance of zero or infinity and noise points have significant depth values, a cut-off filter can be applied to remove pixels laying outside of a predetermined depth range [27]. In RealSense cameras, the SDK is already filtering out the bad points from the sensor while generating the point cloud. However, to tackle the noise problem the distance upper limit was selected to be the sensor height + 200 mm, to ensure the ground can be seen by the sensor. The lower limit is set close to the minimum working distance of D435 RealSense sensor (200mm). This can be expressed as:

$$depth(x, y) = \begin{cases} depth(x, y), & 200 < depth(x, y) < sensorheight + 200 \\ [], & \textit{Otherwise} \end{cases} \quad (2)$$

The following figure demonstrate the effects of depth cut-off filter in noise reduction: the original point cloud is shown on the left (noise areas marked with red), while the resultant one on the right.



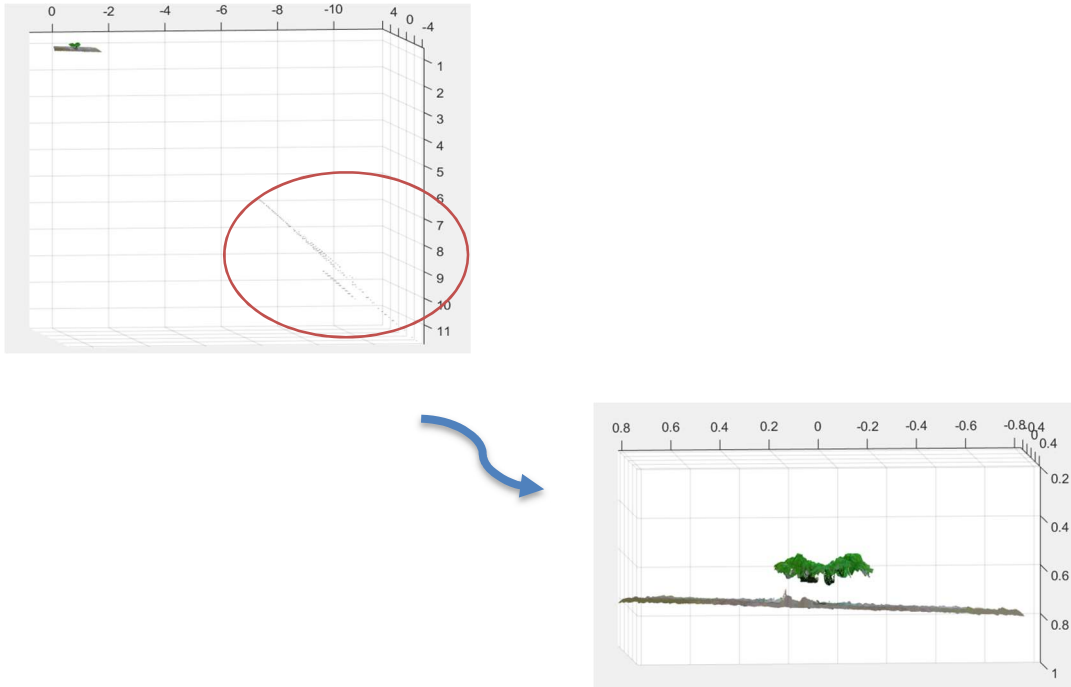


**Figure 23: An example of depth cut-off filter on an image (noise areas have marked with red)**

### 3.3.2 Select the Region of Interest

Due to the distance between the IR camera and the RGB camera in the D435 device, the depth and RGB images are not aligned and need to be aligned while producing point clouds. Furthermore, the depth sensor field of view is larger than the field of view of the RGB sensor. The effect is shown (see Fig. 20). To perform color segmentation, the regions must be observed by the RGB cameras. Furthermore, regions which contain the objects that are not part of measurements must to be excluded. For this reason, a cuboid is specified as a six-element vector of the following form to crop the region of interest (ROI) in the point cloud [82]:

$$ROI = [x_{min}, x_{max}, y_{min}, y_{max}, z_{min}, z_{max}], \quad (3)$$

where  $x_{min}$  and  $x_{max}$  are the minimum and the maximum limits along the x-axis,  $y_{min}$  and  $y_{max}$  are the minimum and the maximum limits along the y-axis, and  $z_{min}$  and  $z_{max}$  are the minimum and the maximum limits along the z-axis respectively.

MATLAB algorithm for obtaining the points within the specified ROI is based on Kd-tree based search algorithm explained in [83]. Let  $G$  be a pixel set in Euclidean space  $E$ . The neighborhood of a pixel  $P$  in this pixel set can be specified as an induced subset of  $G$  including all pixels which their Euclidian distance  $d$  to  $P$  is:

- (a) shorter than determined parameter  $r$   RNS (radius neighbor search)
- (b) or one of the  $k$  shortest.  KNN (k-nearest neighbor search)

k-d tree is the most general method which is utilized to search for neighbors in 3D point cloud. It is a binary tree in which every node is a k-dimensional point. At each non-leaf node, there is a virtual splitting hyperplane that divides the space into two segments. Constructing a k-d tree has a worst complexity of  $O(kn \log n)$ . Using the tree properties of the k-d tree, the neighbor search can be done very efficiently without large portions of the search space. The complexity of the searching algorithm is  $O(\log n)$ , which is much lower than searching in comparison with all the distances to each point [27].

### 3.3.3 Statistical Outlier Removal Filter

For depth sensors such as Intel RealSense, the pixels are denser on flat surfaces than on uneven surfaces. In other words, the pixel on a flat surface has more surrounding pixels in 3D space. Those “connected” pixels are called a “neighborhood” in 3D point cloud, which is similar to the concept of “connectivity” in 2D image processing [27]. Sometimes a dataset can contain some sparse points (noise in most cases) that are unlike the other neighborhood data. These are called outliers and results can be improved by understanding and even removing these outlier values. One of the methods for solving these anomalies can be trimming those which do not meet certain criteria based on a statistical analysis on each point’s neighborhood. Sparse outlier removal filter used in this study is based on the computation of the distribution of point to neighbors’ distances in the input dataset. The mean distance from each point to all its neighbors is calculated. It is assumed that the acquired distribution is Gaussian with a mean and a standard deviation. Thus, those points with mean distances outside an interval defined by the

global distances mean and the standard deviation are considered as out of range data and trimmed from the depth data.

To estimate the features of a point respecting its neighbors, neighborhood points are required to be analyzed to see whether they are good representatives of the underlying sampled surface. The analysis can vary from a simple threshold to performing a more detailed mathematical analysis on the uncertainties in the measured position. Since the method has minimal expectations about the underlying sensing device, it can be applied to any given point cloud data set  $P$ . The majority of point feature representations require an absolute minimum of  $k \geq k_{min}$  neighbors near a query point  $\mathbf{p}_q$  to be determinable. There might be several points in the 2.5 D scans which cannot meet this condition because of the changing density. These are usually the points on high reflective surfaces such as shiny metals. There can also be outliers at the transition between two surfaces because of the occlusions; these are called jump edges, depth discontinuities, or occlusion boundaries. Excluding these points from the point cloud decreases the overall processing time. The proposed solution is based on a statistical analysis of the neighborhood of each point  $\mathbf{p}^k$  and includes the following steps:

1. Firstly, for each point  $\mathbf{p}_q \in P$ , the mean distance  $d$  to its  $k$  closest neighbors is calculated.
2. A distribution assembled over the mean distance space for the entire point cloud  $P$ .
3. Its mean  $\mu_k$  and standard deviation  $\sigma_k$  are estimated.
4. The idea is to keep points such with mean distance  $d$  to the closest  $k$  neighbors similar to the one for the rest of the points. As this describes a measure of the underlying point cloud density surrounding a point, the remaining point cloud  $P^*$  can be determined as follow:

$$P^* = \{\mathbf{p}_q^* \in P \mid (\mu_k - \alpha \cdot \sigma_k) \leq \bar{d}^* \leq (\mu_k + \alpha \cdot \sigma_k)\} \quad (4)$$

where  $\alpha$  is a desirable density restrictiveness factor [84].

The parameters  $\alpha$  and  $k$  are set to 1 and 30 respectively in this work, since experiences with different datasets have approved the applicability of the  $\mu \pm \sigma$  thresholds, with nearly one percent of the points being considered to be noise [85].

## 3.4 Ground Detection

Following point cloud data processing, a plane fitting method is applied to robustly identify the ground plane in the point cloud. This step is required in order to rotate the whole 3D point cloud to make sure that the fitted plane is parallel to xy-plane. In this study, the `pcfitplane()` function from MATLAB Computer Vision Toolbox, which is based on M-estimator SAmple Consensus (MSAC), is used to detect and fit the ground plane. In this algorithm, three points are randomly chosen to fit a plane for one of the iterations. The algorithm fits a plane to a point cloud with the maximum permissible distance from an inlier data point to the plane. It also validates the plane coefficients with orientation limitations.

### 3.4.1 RANSAC

The Random Sample Consensus () algorithm is an iterative method for estimating a mathematical model parameter from a set of experimental data in the presence of outliers [86]. The basic algorithm introduced in 1981 by Fischler and Bolles [87].

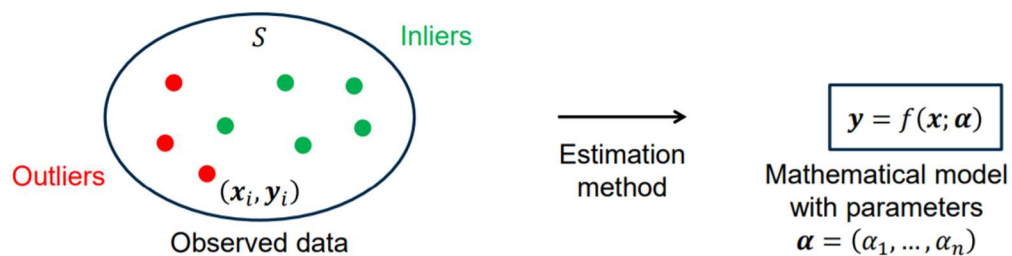


**Figure 24: RANSAC separates the given data into inliers and outliers [86]<sup>14</sup>.**

<sup>14</sup> Reproduced with permission from Thomas Opsahl

For several randomly selected points from the dataset, there is a probability of them all being inliers. The necessary iteration number to find at least one good model is given in equation (5). In this equation,  $N$  is the number of iterations used where at least one good model is found with the probability  $P$ ,  $n$  is the number of selected data points, and  $p$  is the probability of one selected point belonging to the model.  $P = 0.99$  is standard.

$$N = \frac{\log(1-P)}{\log(1-p^n)} \quad (5)$$

The parameter  $p$  is given by Equation (6).

$$p = \frac{M}{D} \quad (6)$$

where  $M$  is the number of inliers in the model and  $D$  is the number of points in the dataset. Usually this ratio is unknown and must be roughly estimated by studying the similar datasets [88].

### 3.4.2 Plane Detection using RANSAC

In computer vision, RANSAC is one of the common algorithms for detecting planes which involves searching for the best plane among point cloud data [89]. The RANSAC algorithm extracts shapes by performing two main steps on an input point cloud: hypothesis generation and hypothesis testing. First, a hypothesis is generated by randomly drawing a sample of  $n$  points and using them to construct a corresponding parameters of shape model. A minimal subset includes the least number of points required to build a unique model.

In the second step, the derived candidate shapes are compared with all points in the data to obtain the score of the shape, where the score corresponds to the number of points that are well-matched by the model. After a certain number of iterations, the shape with the largest number of inliers is extracted and this process is iteratively continued to process the remaining data until the likelihood of obtaining a model with a higher score than the current best model is below a certain threshold ( $T$ ) [90].

RANSAC is a popular algorithm because of the simplicity in concept and for its generality which permits its utilization in a broad range of settings. Furthermore, RANSAC can greatly deal with data including over fifty percent of outliers [91]

There are different versions of RANSAC which have been proposed later to address the problems of the RANSAC and improve its robustness. As an instance, the original RANSAC implementation finds the minimum of the cost function:

$$C_f = \sum_i \rho(e_i^2), \quad (7)$$

where  $e_i$  is the error for the  $i$ th observation, and

$$\rho(e^2) = \begin{cases} 0, & e^2 < T^2 \\ \text{constant}, & e^2 \geq T^2, \end{cases} \quad (8)$$

Torr and Zisserman (2000) demonstrated that selecting the correct value of error threshold ( $T$ ) can be very important and in case of selecting high values for threshold ( $T$ ) the robustness of RANSAC might be very poor. They proposed MSAC (M-estimator Sample Consensus) algorithm which uses a loss function instead of constant thresholds to evaluate the contribution of the inliers based on the point-to-plane distance.

MSAC minimizes the cost function in equation (9) with a robust error function  $\rho_2$ :

$$\rho_2(e^2) = \begin{cases} 0, & e^2 < T^2 \\ T^2, & e^2 \geq T^2, \end{cases} \quad (9)$$

As MSAC improves RANSAC robustness with absolutely no extra cost [92], there is a good reason to use MSAC instead of RANSAC in this research.

### 3.4.3 Plane Equations

To be able to model a plane at least three not collinear points  $P1(x_1, y_1, z_1)$ ,  $P2(x_2, y_2, z_2)$ ,  $P3(x_3, y_3, z_3)$  are necessary. The determinant can be demonstrated by the relation (10):

$$\begin{vmatrix} x & y & z & 1 \\ x_1 & y_1 & z_1 & 1 \\ x_2 & y_2 & z_2 & 1 \\ x_3 & y_3 & z_3 & 1 \end{vmatrix} = 0, \quad (10)$$

Given three points, the plane that contains them is defined as follows:

$$ax + by + cz + d = 0 \quad (11)$$

where a, b and c are plane parameters and d is the distance of the plane from the origin and can be obtained using determinants [63]:

$$a = \begin{vmatrix} 1 & y_1 & z_1 \\ 1 & y_2 & z_2 \\ 1 & y_3 & z_3 \end{vmatrix}, \quad b = \begin{vmatrix} x_1 & 1 & z_1 \\ x_2 & 1 & z_2 \\ x_3 & 1 & z_3 \end{vmatrix}, \quad c = \begin{vmatrix} x_1 & y_1 & 1 \\ x_2 & y_2 & 1 \\ x_3 & y_3 & 1 \end{vmatrix}, \quad d = \begin{vmatrix} x_1 & y_1 & z_1 \\ x_2 & y_2 & z_2 \\ x_3 & y_3 & z_3 \end{vmatrix}, \quad (12)$$

the vector (a,b,c) is a normal .

Given two vectors A and B, the cross-product  $A \times B$  is perpendicular to both A and to B. This can be very helpful in constructing normals [93]. The normal to the plane can be obtained from the cross product of two direction vectors on the plane.

$$\text{normal vector} = (P2 - P1) \times (P3 - P1), \quad (13)$$

Where  $\times$  is the cross product.

The distance between point  $P(x_p, y_p, z_p)$  and plane can be formulated as below [63]:

$$Dist = \frac{|a \times x_p + b \times y_p + c \times z_p + d|}{\sqrt{a^2 + b^2 + c^2}} \quad (14)$$

### 3.5 Camera Misalignment and Slope Correction

This research requires accuracy a within single-digit millimeter range in order to record daily changes of plants (preferably less than 5 mm). Therefore, any camera misalignment or slight slope in greenhouse benches (for letting the flow of water down the slope) can affect the measurement. As can be seen in Figure 25, by simply measuring the distance

between highest point of the same pot at two different positions in the scene to the camera, two very different measurements are obtained. The difference between these two measurements is already more than  $\pm 5$  mm which is the beyond the target in this project. In Figure 25(a), the position of the pot is closer to the centre of the camera while in Figure 25(b) the pot is farther.

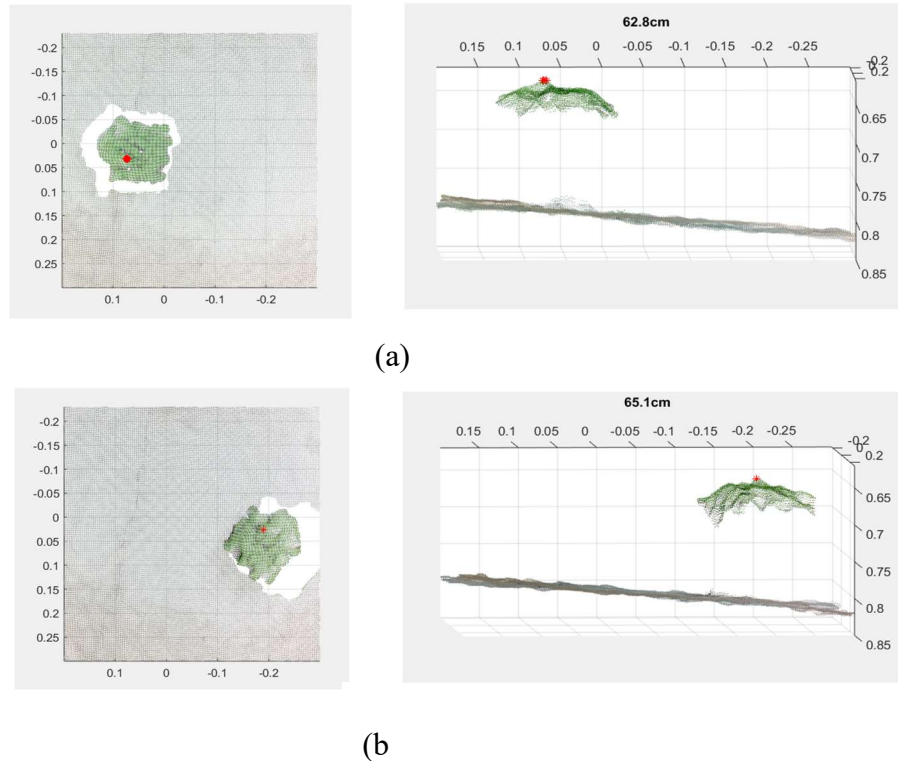


**Figure 25: Measuring highest point at two different positions (a) closer to the centre of camera (b) closer to the corner of image. The actual distance of the highest point from camera measured manually and is about 62.9 cm.**

In this regard, an algorithm is needed to perform a 3D transformation of the point cloud. Having the normal vector of the current plane obtained in ground detection stage and the reference vector for z-axis  $[0,0,1]$ , the rotation angle, rotation axis, and finally, rotation matrix can be calculated using the axis-angle approach.



### 3.5.1 Rotation Matrix from Axis and Angle

According to Euler rotation theorem, each rotation in three dimensions is described by its axis (a vector along this axis is unaltered by the rotation), and its amount of rotation (angle).

Having the normal vector of the current plane and the reference vector, the rotation angle and rotation axis can be calculated. Ultimately a rotation matrix can be generated using the axis-angle approach. In this method, the angle between the two vectors is found using dot product and then a proper rotation axis about which this angle is subtended is calculated using the cross product.

Given a unit vector  $\mathbf{u} = (u_x, u_y, u_z)$ , where  $u_x^2 + u_y^2 + u_z^2 = 1$ , the rotation matrix will be formulated as below [94]:

(15)

$$R = \begin{bmatrix} \cos \theta + u_x^2(1 - \cos \theta) & u_x u_y(1 - \cos \theta) - u_z \sin \theta & u_x u_z(1 - \cos \theta) + u_y \sin \theta \\ u_y u_x(1 - \cos \theta) + u_z \sin \theta & \cos \theta + u_y^2(1 - \cos \theta) & u_y u_z(1 - \cos \theta) - u_x \sin \theta \\ u_z u_x(1 - \cos \theta) - u_y \sin \theta & u_z u_y(1 - \cos \theta) + u_x \sin \theta & \cos \theta + u_z^2(1 - \cos \theta) \end{bmatrix}$$

Where  $\theta$  is the angle of rotation about an axis in a direction of  $\mathbf{u}$ . This can be briefly written as:

$$R = (\cos \theta)\mathbf{I} + (\sin \theta)[\mathbf{u}]_{\times} + (1 - \cos \theta)(\mathbf{u} \otimes \mathbf{u}), \quad (16)$$

where  $\mathbf{I}$  is the identify matrix, and

$\otimes$  is the outer product,

$$\mathbf{u} \otimes \mathbf{u} = \mathbf{u}\mathbf{u}^T = \begin{bmatrix} u_x^2 & u_x u_y & u_x u_z \\ u_x u_y & u_y^2 & u_y u_z \\ u_x u_z & u_y u_z & u_z^2 \end{bmatrix} \quad (17)$$

and  $[\mathbf{u}]_{\times}$  is the cross product of  $\mathbf{u}$ :

$$[\mathbf{u}]_{\times} = \begin{bmatrix} 0 & -u_z & u_y \\ u_z & 0 & -u_x \\ -u_y & u_x & 0 \end{bmatrix} \quad (18)$$

Based on the Right-hand rule and  $\theta > 0$ , if the three-dimensional space is right-handed, the rotation is counterclockwise when  $\mathbf{u}$  points towards the observer and considered as a positive rotation.

The whole point cloud is rotated by a rotation matrix. Figure 26 demonstrates the example was shown in Figure 25 after performing rotation. The ground level in this new point cloud is roughly parallel to the x-y plane in both cases.

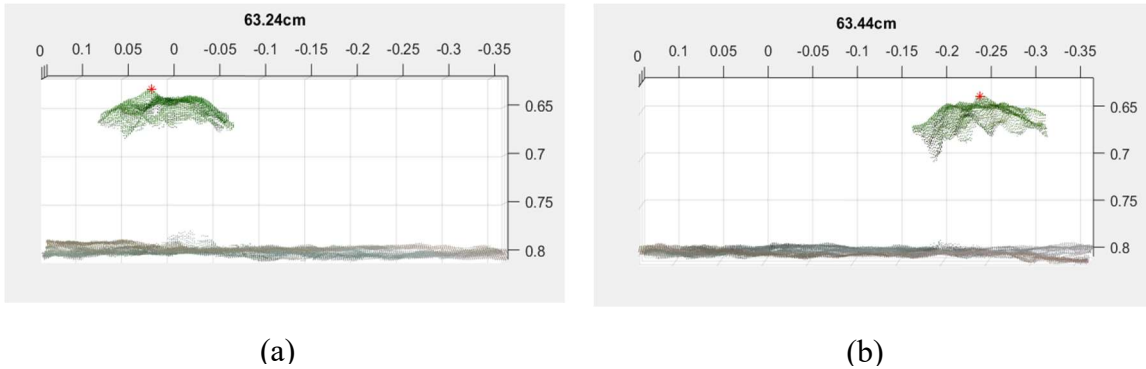


**Figure 26: (a) The proposed algorithm slightly reduced the depth accuracy when the highest point is in the middle (Figure (25(a))), but it keeps the tolerance in acceptable range. (b) On the other hand, the algorithm improved the depth measurement when pot was located at second position (Figure (25(b))).**

This ground calibration is not necessary each time because the rotation matrix can be saved and used in each acquisition. Recalibration is needed only if the table or camera position changed with respect to ground.

### 3.6 Background Removal and Plant Segmentation

After generating and preprocessing of the point clouds, the next step is segmentation. In this stage, the goal is to separate vegetation pixels from the background pixels.

Identification of greenness is directly impacted by the quality of the plant image. Different factors can affect the quality of the plant image captured outdoors such as illumination, the color range of the leaves and complexity of the background [95]. Both depth and color information are utilized in this stage to efficiently and robustly segment the biomass pixels which are higher in green color and expected to be in specific height range.

Color segmentation based on only RGB channels is prone to change because of the complexity of illumination conditions (e.g. shadows). The HSV color space is therefore more useful in green pixel segmentation because of its lower sensitivity to illumination conditions [27].

The algorithm used for automatic detection of pixels corresponds to basil plants from is organized as follows: First, the point cloud RGB color values were transformed to HSV color space to make the algorithm less sensitive to lighting variations. Second, thresholding is employed based on HSV channels and the depth region of interest to segment the green leaves. Most of the background elements were eliminated in this stage.

### 3.6.1 HSV Color Space

RGB (red, green, and blue) is a color space that is commonly used, but sometimes it is preferable to use HSV. HSV consists of three components (Hue, Saturation, and Value). Hue determines the intrinsic property of the color. Saturation describes the purity of the color. The third component of the HSV, Value measures the brightness of the color [96].

Hue is the specification of a vision based on which an area is close to one of the red, yellow, green and blue sensed colors, or to a mixture of two of them. It can be represented in angle on the circle. While a circle consists of 360 degrees of rotation, the normalized hue ranges from 0 to 255, starting from red. Saturation is a measurement of the departure of a hue from achromatic, i.e., from white or gray and varies from 0 to 255. The lower the saturation value means more gray in the color. Finally, the Value channel

measures the departure of a hue from black. Value varies from 0 to 255, with 0 being fully dark and 255 being fully bright [97] .

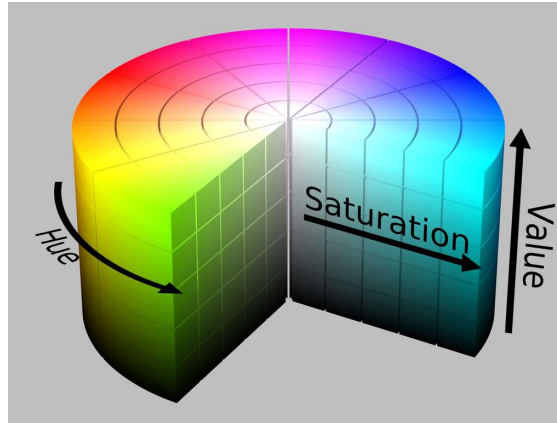


**Figure 27: Illustration of the HSV color space [98]<sup>15</sup>**

HSV has been widely used in computer vision projects. Using HSV color space for segmentation has some advantages over using the RGB including:

- 1) Hue remains constant in specific types of highlights, shading, and shadows.
- 2) Segmentation is simpler in HSV because the segmentation is mostly performed on hue dimension which is not the case in RGB [96]. In MATLAB, hue, saturation and value range from 0 to 1.0. Therefore, RGB values are required to be divided by 255:

$$R = R/255 \tag{19}$$

$$G = G/255 \tag{20}$$

$$B = B/255 \tag{21}$$

---

HSV\_color\_solid\_cylinder.png: SharkDderivative work: SharkD Talk [CC BY-SA 3.0(<https://creativecommons.org/licenses/by-sa/3.0>)]

### 3.6.2 RGB to HSV Algorithm

The algorithm used for conversion from RGB space to HSV space is based on [99] and can be summarized as follows:

Input: R, G and B, each on a domain [0, 1]

Output: The equivalent H, S, and V, each on the range [0, 1]

1. Let  $V = \max(R, G, B)$
2. Let  $X = \min(R, G, B)$
3.  $S = \frac{V-X}{V}$  ; if  $S = 0$  return;
4. Let  $r = \frac{V-R}{V-X}$ ;  $g = \frac{V-G}{V-X}$ ;  $b = \frac{V-B}{V-X}$
5. If  $R = V$  then  $H = (\text{if } G = X \text{ then } 5 + b \text{ else } 1 - g)$ ;  
     If  $G = V$  then  $H = (\text{if } B = X \text{ then } 1 + r \text{ else } 3 - b)$ ;  
     else  $H = (\text{if } R = X \text{ then } 3 + G \text{ else } 5 - r)$ ;
6.  $H=H/6$ ;

An example image of Hue, Saturation and Value channels for an image is as follows:

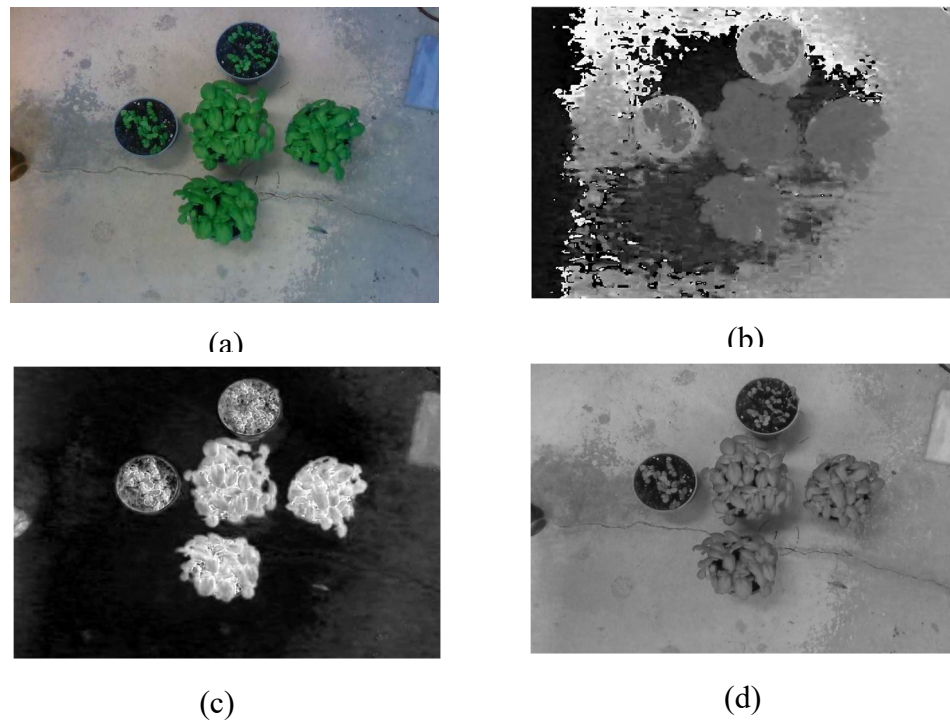


**Figure 28: RGB to HSV conversion example (a) RGB image (b) H channel image (c) S channel image (d) V channel image**

### 3.6.3 Color and Depth Segmentation

As can be seen in Figure 28(b), some of the foreground and background pixels in the training image had the same hue values. To reduce the impact of the background complexity on segmentation and consequently height measurement, both color and depth segmentation are used in this procedure. First, a depth range is defined to constrain the number of points that need to be analysed for height measurement. The height dimension of the pot is selected as one threshold. The maximum growth of a basil plant at the packaging stage is considered as another height threshold (approximately 30 cm from the edge of plants for basils). This first depth thresholding simplifies the task of greenness segmentation of plants.

The purpose of color-based segmentation in this project is to extract the pixels corresponding to the plants. In agriculture, most images are captured in the greenhouse or other outdoor environments. Recognition of green leaves in natural scenes can be challenging due to the complexity of the background and varying light conditions. HSV (Hue-Saturation-Value) color space is considered one of the most reliable color spaces in green plants extraction from the background. The plant hue values are almost invariant under different light intensity [27].

Identification of greenness based on HSV color space in this project includes the following steps: First, hue histograms are generated based on the training image (Fig.28). Hue threshold values are selected based on the plant color range. Generally, the hue values of green color vary from 60 to 180 [95]. Knowing this, upper and lower threshold values are selected first based on the hue histogram analysis and then improved by observing the segmentation. The threshold values are used later to segment basil leaves in the point clouds. Thresholding further is processed based on the following assumptions: pixels within [lower, upper] hue and within defined depth range is set to 1 and the remaining pixels are removed. By this strategy, most of the background pixels are eliminated compared with the leaves pixels. (Figure 29).

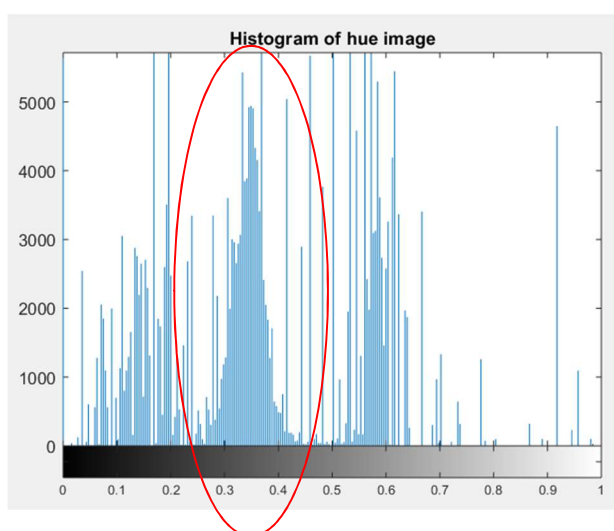


**Figure 29: Histogram of hue image. Hue values of green color is approximately between 0.25 and 0.45 (marked with red)**

### 3.7 Plant Height Estimation

The plant height results are determined by subtracting the minimum depth value of the vegetation points from the height of the camera and the height of the pot.

$$\text{Plant height}(h) = (z_1 - z_2) - z_3 \quad (22)$$

Where  $h$  is plant height from the edge of the pot to the highest point of the plant,  $z_3$  is the  $z$ -value(s) for which the rest of the points of the point cloud are below,  $z_1$  is the distance of the camera from the ground measured manually, and  $z_2$  is the height of the plant pot (Figure 30).

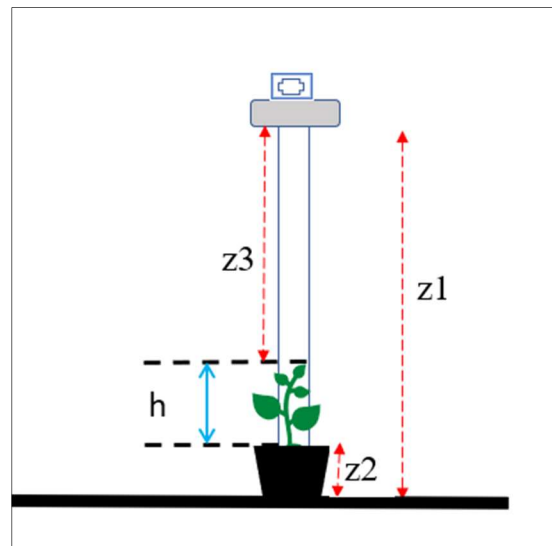


**Figure 30: Plant height measurement.  $h$ : plant height,  $z_3$ :  $z$ -value(s) for which the rest of the points of the point cloud are below,  $z_1$ : the distance of the camera from the ground measured manually, and  $z_2$ : the height of the plant pot**



## 4 Experimental Results

The developed algorithms were tested by conducting growth analysis of the target plant (basil). The data used in this work were obtained in the Vineland Research and Innovation Centre located in Lincoln in Canada County. The crop plants were started in the greenhouse within one week and two weeks before data acquisition.

To test different light conditions, part of the experiment was done in an office under typical office conditions with some ambient light coming from the window (Figure 31(a)) and the rest was done in the hangar building under a ceiling light (Figure 31(b)). Both grounds were made from concrete and had some slope.



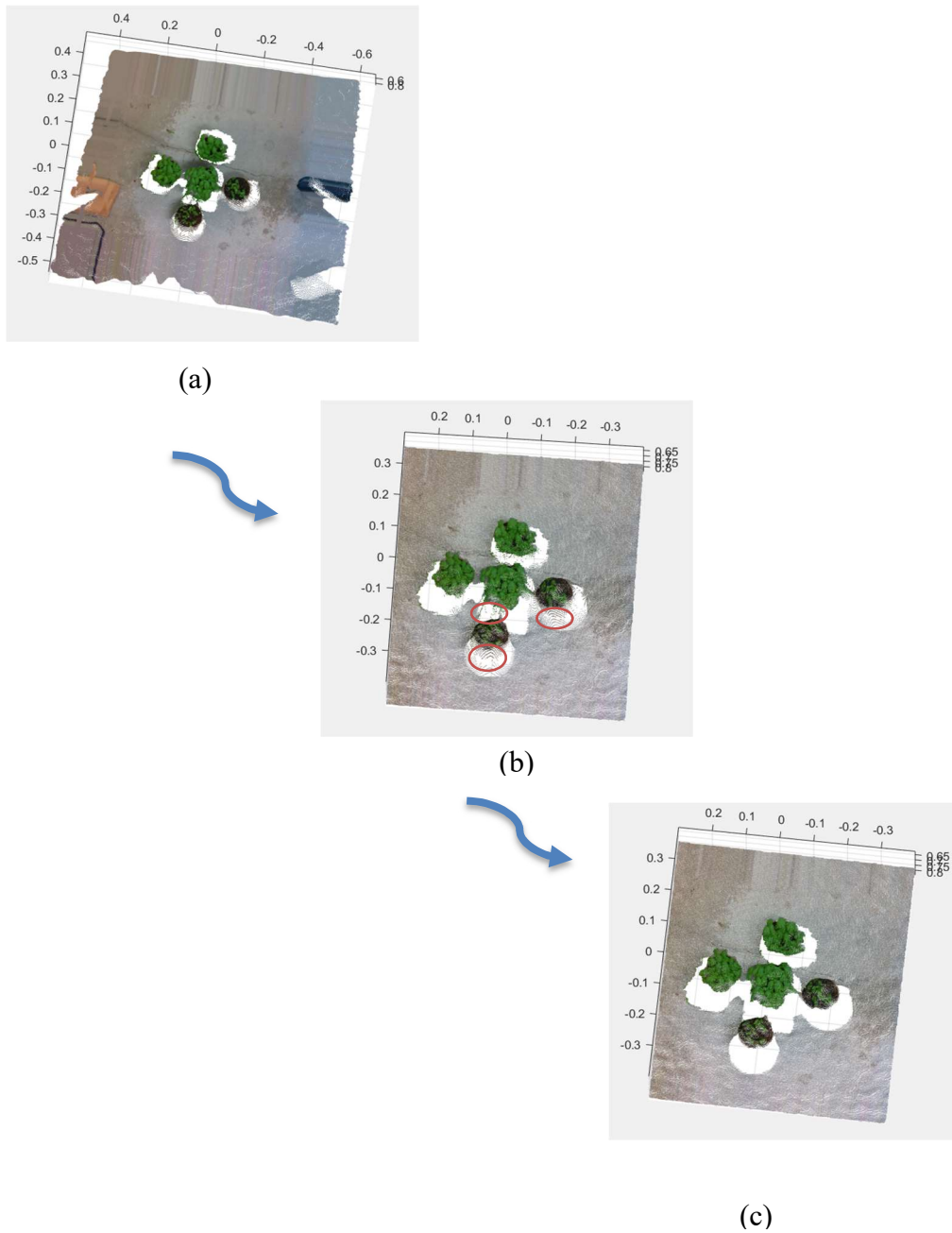
**Figure 31: The 3D imaging experiments for sample plants were carried out in two environments: (a) an indoor office with some ambient light coming from the window (b) hangar building under a ceiling light (no window)**

Data were acquired for each individual pot and for a group of plants. Frequent measurements were performed along the growth cycle. Each individual plant was placed on the ground at the center of the camera's FOV because best performance is usually obtained in this position. Then the combination of plants randomly placed in the scene right after and the maximum height was calculated. Height of each plant was also

measured manually by two persons considering the highest tip of the plants to the edge of the pot. Plants were measured located in different positions one by one or in a group. The average of the two human measurements has been considered as ground truth. Data from day 1 to 15 was captured in the office while the rest of the experiments were conducted in the hangar building to examine the performance of the camera in different light conditions and ground slopes.

## 4.1 Preprocessing Results

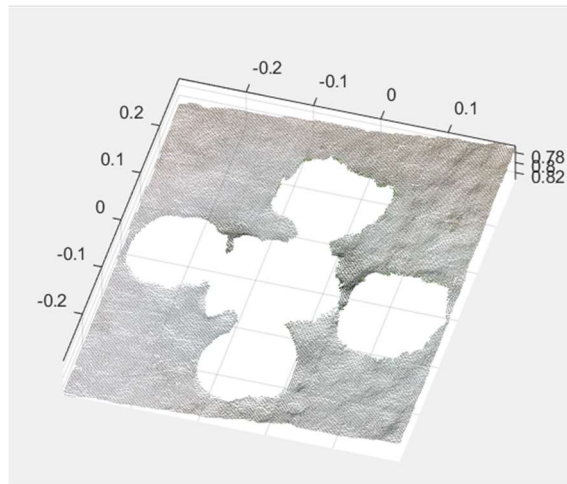
A point cloud was generated from color and depth images. The cut-off filter applied to eliminate noise. Fig. 32(a) demonstrates the point cloud after initial noise reduction. Figure 32(b) illustrates the point cloud after cropping based on a defined region of interest. The part (b) of the figure also presents a point cloud dataset  $P$  containing several areas with lower point densities (marked with red circles). The right part of the figure presents the remaining point cloud  $P^*$  (see section 3.3.3), after the removing sparse points being situated in sparse density regions.



**Figure 32: An example of point cloud preprocessing: (a) The original image (b) after selecting region of interest (c) after Statistical Outlier Removal filtering**

## 4.2 Plane Detection Results

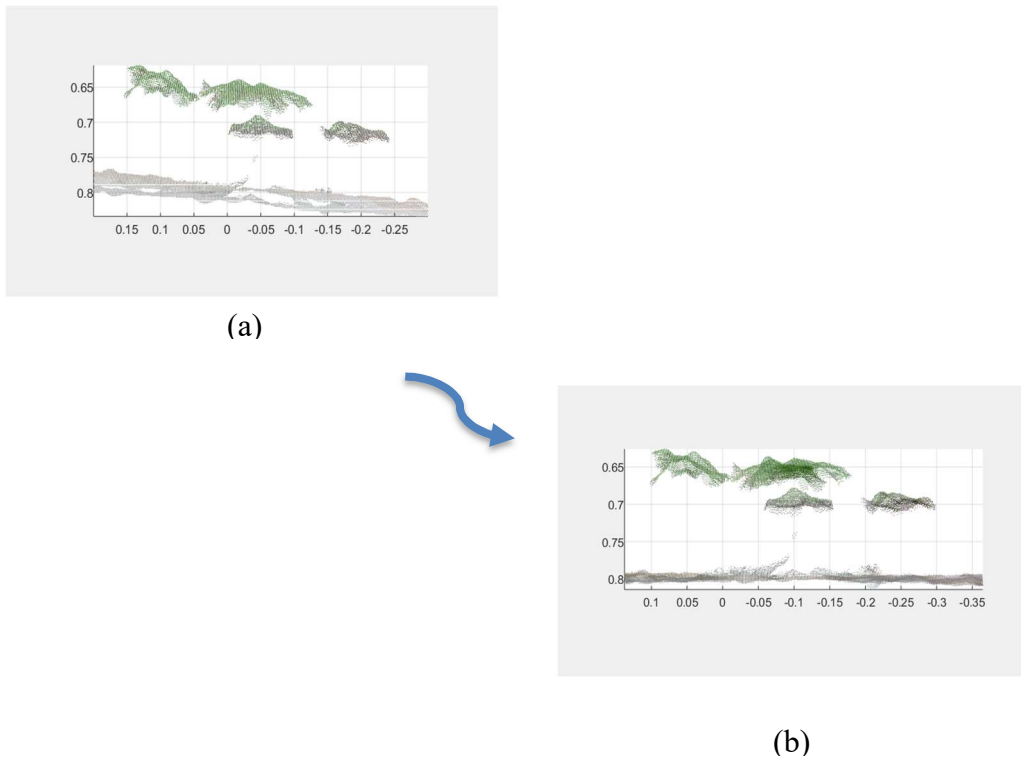
In this work, input parameters were set in a way that each point within 2cm from the ground plane is considered to be an inlier. Also, the normal direction of the plane is checked to be roughly pointing upward along the Z-axis with maximum 5-degree angular distance. The other parameters such as the maximum number of random trials for finding the inliers and confidence percentage for finding the maximum number of inliers remained as default: 1000 and 0.99 respectively. The output of this algorithm returns a geometrical model that defines the plane.



**Figure 33: An example of ground plane detection**

## 4.3 Correction Results

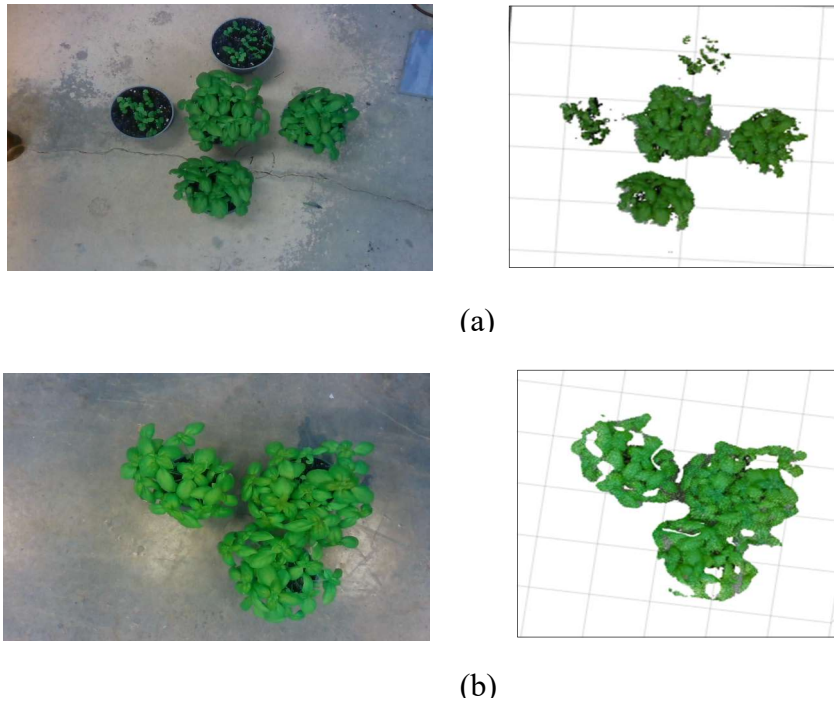
In our experiment, we calibrated our ground two times. The first calibration was performed in the office and the second when we moved the system to the hangar building. Figure 34(a) and 34(b) show an example point cloud before and after the correction using the proposed method.



**Figure 34: An example of camera misalignment and slope correction for office environment (a) before correction (b) after correction**

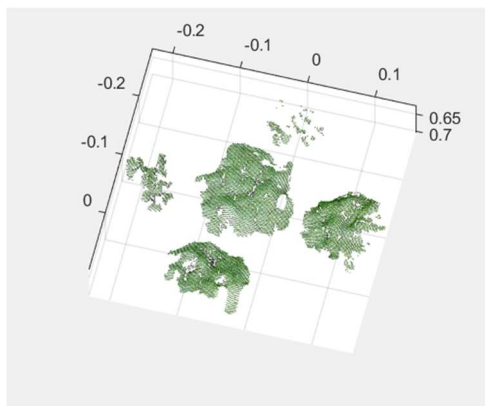
#### 4.4 Image Segmentation Results

Fig 35(a) & 35(b) shows the examples of segmentation results for training and test point cloud data sets respectively.



**Figure 35: Plant identification (a) training (in the office) (b) test (in the hangar)**

Although the best situation is to identify the green pixels from the scene only by their hue values, sometimes the changing leaf color or different background elements make the green pixel detection a challenging task. Therefore, in such cases, it might be necessary to analyze the distributions of hue, saturation and value components of the image [95].



**Figure 36: An example of green plant segmentation based on hue and saturation components**

## 4.5 Plant Height Measurement Results

An example height measurement is shown in Figure 37. The detected highest tip of the canopy used to calculate the plant height has marked with red. Plant height in centimeters is shown on the figure.

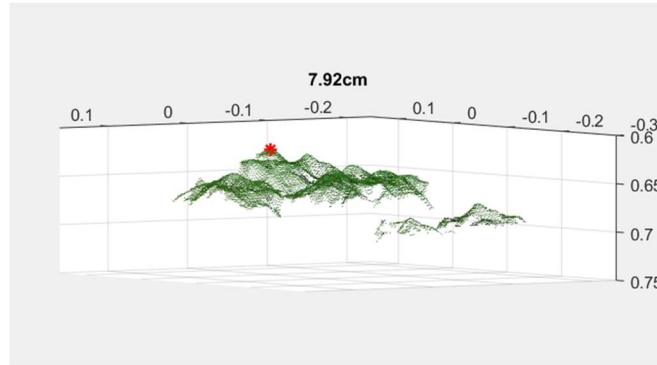


**Figure 37: Demonstration of a maximum point of the canopy (marked with red)**

For each individual pot and group of plants, estimated heights are plotted against actual heights (Fig. 36). To evaluate height estimation, coefficient of determination ( $R^2$ ), root mean square error (RMSE) are used. The mean absolute error (MAE) is also calculated since it has been proved that it can provide more reliable measurement of average error than RMSE, particularly when estimation results acquired from various size samples are compared [58].

$$RMSE = \sqrt{\text{mean}(\text{reference height} - \text{estimated height})^2} \quad (23)$$

$$MAE = \text{mean}(|\text{reference height} - \text{estimated height}|) \quad (24)$$

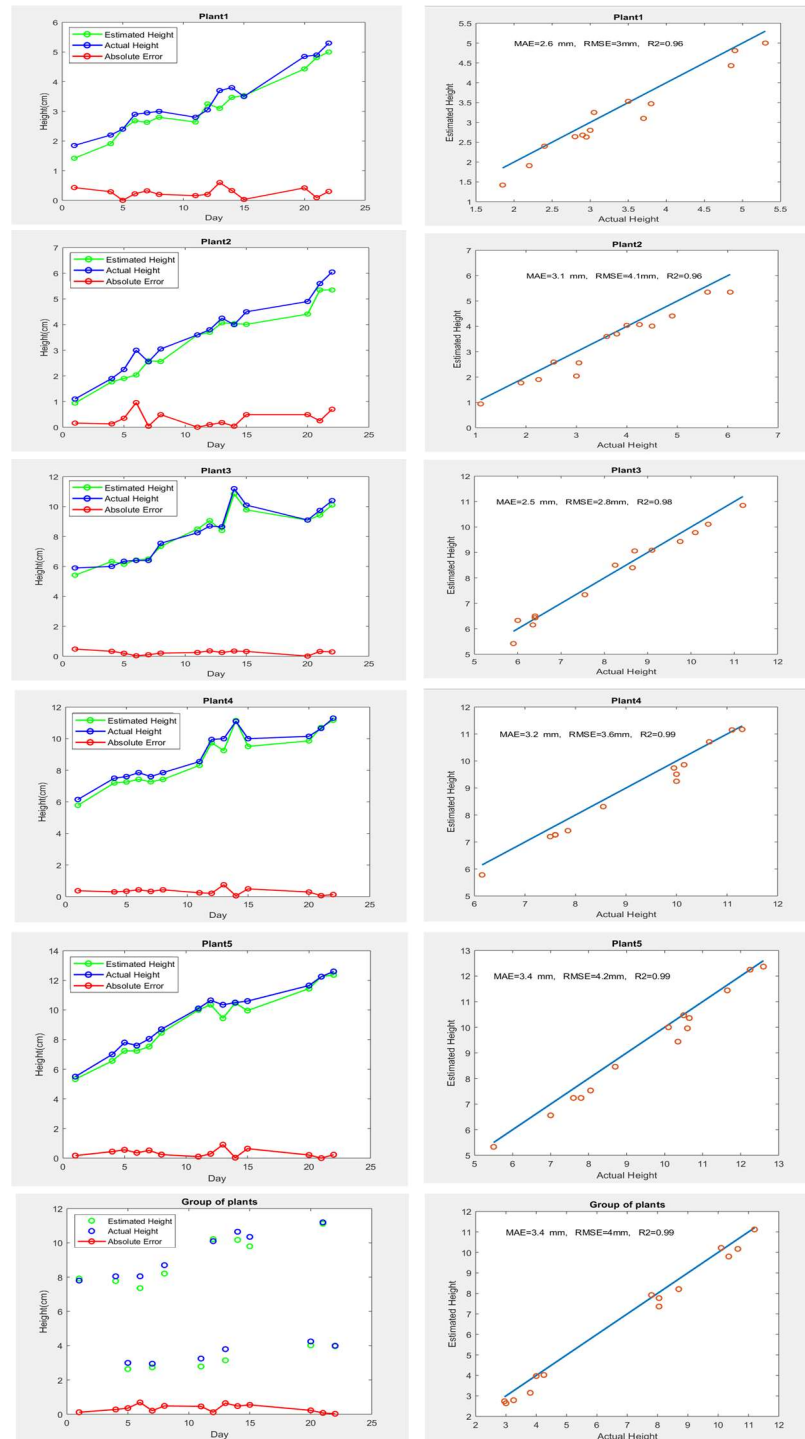


**Figure 38: Comparison between plant height derived from RealSense D435 camera measurements with plant height measured manually (For individual Basils (rows 1 to 5) and for group of Basils (row 6) )**



As can be inferred from results, there are strong linear correlations and low average errors between estimated and actual values. The height of individual plants (plants 1 to 5) yielded a correlation  $R^2 = 0.96$  to  $0.99$  to the reference measurements. The RMSE reached 2.8-4 mm, while the MAE was 2.5-3.4mm. For group of plants, a correlation of  $R^2 = 0.99$  was reached with an RMSE of about 4 mm and a MAE lying at 3.4mm.

The results demonstrated that the proposed method can successfully measure the height of basil in different environments and in different layouts. This can also indicate that resolution and accuracy of height map from D435 Intel RealSense allow a good estimation of height for leafy vegetables similar to basils. However, as it can be inferred from the charts, results obtained from basils during the later growth period (plant 3 to 5) were more correlated to the manual measurement than those in early growth stages because of the bigger surface area which makes the detection of highest point simpler for both human and camera.

## 5 Conclusion

### 5.1 Introduction

In this thesis, different problems related to automated plant growth analysis in greenhouses have been investigated. We have shown that the proposed system can be reliably used for comparing the height of different sizes of leafy plants such as basil over time, and can autonomously provide results as good human measurement in various environmental conditions. This Chapter contains the summary of the thesis contents, conclusions that have been reached based on the conducted experiments, main contributions of the thesis, and potential future work suggestions that can be done based on this thesis work.

### 5.2 Summary

Plant height is related to the plant yield and rate of growth. It can be also utilized as an indicator of water stress in smart irrigation applications. The automation of plant height measurement is essential in making this process more efficient, accurate and reproducible. Systems based on point-based sensors, light curtain arrays and two-dimensional sensing for plant height measurement suffer from certain shortcomings. With the development of computer technology and imaging devices, 3D data was used to achieve more precise measurement and more detailed information to characterize the plant spatial distributions. Previous researches showed that Microsoft Kinect v2 3D sensor has huge potentials in agriculture applications including growth measurement of leafy vegetables, benefited from its strong robustness while it has a low price. However, it is discontinued. Intel RealSense sensors seem to be a good replacement for Kinect v2 sensors as they have high resolution and accuracy as well as a wide field of view. This sensor is based on active stereo technology and can be used for both indoor and outdoor applications under a variety of light conditions. This study presents an automated and non-destructive method for accurate crop plant height measurement using an Intel RealSense D435 depth sensor.

The first objective of this thesis was exploring a variety of 3D imaging technologies, deciding on the suitable technology for the current application, and finding proper equipment considering aspects such as the camera price, required resolution, accuracy, field of view, sensitivity to light, etc. In this regard, in chapter 1 and 2, fundamental concepts related to computer vision and different 3D sensing technologies were introduced. Furthermore, previously proposed methods for plant growth and plant height measurement were reviewed and the thesis objectives were stated. Based on an analysis of the greenhouse environment, previous researches on plant growth measurement, and after comparing the pros and cons of each 3D sensing technologies, active stereo selected as a suitable match with the current application. For these reasons, the Intel RealSense D435 camera was used to obtain depth and color image.

The second objective of this project was to develop algorithms and strategies for identifying the plant in the image, acquiring a region of interest depth data to understand the crop's distance from the camera and extract plant height. Chapter 3 contains all the methods and algorithms used to identify the plant as well as demonstration and evaluation of results. The contents of this chapter are summarized as follows: 3D point cloud generated from RGBD camera, and various preprocessing steps are then implemented for data filtering and data cleaning including noise reduction, outlier elimination, and region of interest selection. Due to the high required accuracy, a ground calibration method introduced to correct any camera misalignments and ground slopes in the surface which plant(s) is located on. For this reason, the major plane detected by finding the plane coefficients using RANSAC-based method. Then, ground plane normal used to correct any camera misalignments and ground slopes. In the next step, plants were discriminated from the background using a robust method that uses both height and color information. To reduce the effect of light on the measurement, the experiment's images were analysed in HSV color space. Plant height was estimated by finding the highest point of plants.

To validate reliability and robustness to various changes in the environment including light and slope of the ground, the proposed method was tested on five basil pots in two different environment and light conditions using a MATLAB developed program. Plant height was well estimated and high correlations and low average errors were obtained between estimated and actual values.

### 5.3 Conclusions

This research aimed to propose an accurate plant height measurement in greenhouses using commercial sensors. The following conclusions can be made based on the results of this thesis:

1. Results demonstrated that D435 can successfully track the daily growth of leafy vegetables such as basil plants with less than  $\pm 5\text{mm}$  mean absolute error in comparison with a human. Our proposed algorithm to measure a plant's height can be applied for other plants that have characteristics similar to basil.
2. The proposed algorithm for ground calibration can successfully correct the issue of the slopes in grounds and camera misalignments and as a result, improve the accuracy of the plant height measurement.
3. Color segmentation in HSV color space can detect plants in both environments due to its insensitivity to illumination changes. Furthermore, the combination of depth and color provided faster and more accurate detection of vegetation points on the scene because of the smaller number of points and also removing undesired areas. However, analysing other HSV components of the scene might be needed to improve the quality of segmentation especially in edges and occluded leaves areas.

### 5.4 Contributions

The principal contributions of this thesis are as follows:

- i. The possibility of using D435 RealSense camera for plant height measurement application was investigated and results demonstrated.
- ii. A MATLAB based program to perform identification and height measurements of plants was developed and its feasibility was confirmed by implementing this program for several sample images taken from basil plants.
- iii. A method for ground calibration (including plane detection and slope and misalignment correction) was proposed which provides the feasibility of an easy calibration with different growing beds. It can be used in various relevant experiments as a mean of calibration.

## 5.5 Discussions & Future Work

Based on experiments obtained in this study, the following suggestions are made for future work.

In the ground detection algorithm, the assumption is that the major plane is ground. In a real greenhouse environment, it might fail to detect the correct plane because of the complexity of the background and existence of multi-step scenes. To improve the reliability of the ground plane algorithm, a proposed solution might be to determine the 3D coordinates of three points that are located on the ground plane using a calibration object. For example, in [63], three circles with known diameter were located on the ground plane and used to build the ground plane equation in the way that points P1, P2 and P3 described in plane equation section (3.4.3) correspond to the centers of three circles.

In developing algorithms an effort has been made to keep the proposed method general for use in many different applications of plant height measurement without changes or with minor modifications. However, the proposed method needs to be tested on different plant structures especially on those with sharp tips or little blossoms. In some plant types, it might be needed to increase the resolution to the highest possible resolution (1280 x 720) or also use two or more cameras acquiring images from different view angles at the

same time. Although this might provide a denser point cloud to improve plant segmentation and reduce image occlusions, it will probably increase the processing time due to the larger number of points need to be processed.

The other strength of this system is that the results have been obtained via direct sensing and not after post-processing. However, the proposed method might need more investigations on processing time per image in different resolutions to consider the option of using the system on a moving boom.

Lastly, note that experiments were conducted in a lab-based environment to ensure conditions were ideal for the camera after finding poor environmental effects on depth sensing at commercial greenhouses. Future work will require more effort to ensure the system operates in a commercial setting.

## 5.6 Abbreviations

**2D:** Two-dimensional

**3D:** Three-dimensional

**ISP:** Image Signal Processor

**IR:** infrared

**FoV:** field of view

**HSV:** hue-saturation-value

**KNN:** k-nearest neighbor

**LC:** Light Curtain

**LiDAR:** Light Detection and Ranging

**MAE:** Mean Absolute Error

**MRE:** Mean Relative Error

**MSAC:** M-estimator Sample Consensus

**PMD:** Photonic Mixer Detector

**RANSAC:** Random Sample Consensus

**RGB:** Red–Green–Blue

**RGBD:** A combination of an RGB image and its corresponding depth image

**RMSE:** Root Mean Square Error

**RNS:** Radius Neighbor Search

**ROI:** Region of Interest

**SfM:** Structure from Motion

**ToF:** Time-Of-Flight

## References or Bibliography

- [1] K. Lin, J. Chen, H. Si, and J. Wu, “A Review on Computer Vision Technologies Applied in Greenhouse Plant Stress Detection BT - Advances in Image and Graphics Technologies,” in *Chinese Conference on Image and Graphics Technologies*, Springer Berlin Heidelberg, 2013, pp. 192–200.
- [2] D. Shrestha, B. Steward, T. Kaspar, and P. Robert, “Determination of early stage corn plant height using stereo vision,” in *6th International Conference on Precision Agriculture and Other Precision Resources Management, Minneapolis, MN*, 2002, pp. 1382–1394.
- [3] T. S. Colvin, S. Arslan, and D. W. Meek, “Yield Monitors, Combines, and Their Interactions,” 1999.
- [4] D. Story and M. Kacira, “Design and implementation of a computer vision-guided greenhouse crop diagnostics system,” *Machine Vision and Applications*, vol. 26, no. 4, pp. 495–506, 2015.
- [5] Y. Hu, L. Wang, L. Xiang, Q. Wu, and H. Jiang, “Automatic non-destructive growth measurement of leafy vegetables based on kinect,” *Sensors (Switzerland)*, vol. 18, no. 3, Mar. 2018.
- [6] Y. Jiang, C. Li, and A. H. Paterson, “High throughput phenotyping of cotton plant height using depth images under field conditions,” *Computers and Electronics in Agriculture*, vol. 130, pp. 57–68, Nov. 2016.
- [7] K. P. Constantino, E. J. Gonzales, L. M. Lazaro, E. C. Serrano, and B. P. Samson, “Plant height measurement and tiller segmentation of rice crops using image processing,” in *Proceedings of the DLSU Research Congress*, 2015, vol. 3, pp. 1–6.



- [8] W.-T. Chen, Y.-H. F. Yeh, T.-Y. Liu, and T.-T. Lin, “An automatic plant growth measurement system for plant factory,” *IFAC Proceedings Volumes*, vol. 46, no. 4, pp. 323–327, 2013.
- [9] R. T. Furbank and M. Tester, “Phenomics—technologies to relieve the phenotyping bottleneck,” *Trends in plant science*, vol. 16, no. 12, pp. 635–644, 2011.
- [10] H. T. Cao, “A Low-cost Depth Imaging Mobile Platform for Canola Phenotyping,” 2018. [Online]. Available: <http://hdl.handle.net/10388/8526>.
- [11] S. Henderson, “Improving Greenhouse Irrigation Through A Sensor-Based Decision Support System,” The University of Guelph, 2017.
- [12] T. W. Sammis, D. Smeal, and S. Williams, “Predicting Corn Yield Under Limited Irrigation Using Plant Height,” *Transactions of the ASAE*, vol. 31, no. 3, pp. 830–837, 1988.
- [13] T. Helmer, D. L. Ehret, and S. Bittman, “CropAssist, an automated system for direct measurement of greenhouse tomato growth and water use,” *Computers and Electronics in Agriculture*, vol. 48, no. 3, pp. 198–215, Sep. 2005.
- [14] M. Minervini, H. Scharr, and S. A. Tsafaris, “Image analysis: the new bottleneck in plant phenotyping [applications corner],” *IEEE signal processing magazine*, vol. 32, no. 4, pp. 126–131, 2015.
- [15] H. Zhao, L. Xu, H. Jiang, S. Shi, and D. Chen, “High Throughput System for Plant Height and Hyperspectral Measurement,” *International Archives of the Photogrammetry, Remote Sensing and Spatial Information Sciences*, vol. 42, p. 3, 2018.
- [16] S. Schwartz, “An overview of 3D plant phenotyping methods,” *PHENOSPEX*, 2015. [Online]. Available: [phenospex.com/blog/an-overview-of-3d-plant-phenotyping-methods/](http://phenospex.com/blog/an-overview-of-3d-plant-phenotyping-methods/). [Accessed: 21-Apr-2019].

- [17] C. Mccarthy, N. Hancock, and S. Raine, “Applied machine vision of plants: A review with implications for field deployment in automated farming operations,” *Intelligent Service Robotics*, vol. 3, pp. 209–217, Oct. 2010.
- [18] F. Fiorani and U. Schurr, “Future Scenarios for Plant Phenotyping,” *Annual Review of Plant Biology*, vol. 64, no. 1, pp. 267–291, Apr. 2013.
- [19] L. Li, Q. Zhang, and D. Huang, “A review of imaging techniques for plant phenotyping,” *Sensors*, vol. 14, no. 11, pp. 20078–20111, 2014.
- [20] D. Li, L. Xu, X. S. Tang, S. Sun, X. Cai, and P. Zhang, “3D imaging of greenhouse plants with an inexpensive binocular stereo vision system,” *Remote Sensing*, vol. 9, no. 5, May 2017.
- [21] R. N. Lati, S. Filin, and H. Eizenberg, “Estimation of plants’ growth parameters via image-based reconstruction of their three-dimensional shape,” *Agronomy Journal*, vol. 105, no. 1, pp. 191–198, 2013.
- [22] L. Busemeyer, D. Mentrup, K. Möller, E. Wunder, K. Alheit, V. Hahn, H. Maurer, J. Reif, T. Würschum, and J. Müller, “BreedVision—A multi-sensor platform for non-destructive field-based phenotyping in plant breeding,” *Sensors*, vol. 13, no. 3, pp. 2830–2847, 2013.
- [23] P. Andrade-Sanchez, M. A. Gore, J. T. Heun, K. R. Thorp, A. E. Carmo-Silva, A. N. French, M. E. Salvucci, and J. W. White, “Development and evaluation of a field-based high-throughput phenotyping platform,” *Functional Plant Biology*, vol. 41, no. 1, pp. 68–79, 2014.
- [24] A. A. Farooque, Y. K. Chang, Q. U. Zaman, D. Groulx, A. W. Schumann, and T. J. Esau, “Performance evaluation of multiple ground based sensors mounted on a commercial wild blueberry harvester to sense plant height, fruit yield and topographic features in real-time,” *Computers and electronics in agriculture*, vol. 91, pp. 135–144, 2013.

- [25] D. Fanourakis, C. Briese, J. F. J. Max, S. Kleinen, A. Putz, F. Fiorani, A. Ulbrich, and U. Schurr, "Rapid determination of leaf area and plant height by using light curtain arrays in four species with contrasting shoot architecture," *Plant Methods*, vol. 10, no. 1, Apr. 2014.
- [26] J. M. Montes, F. Technow, B. S. Dhillon, F. Mauch, and A. E. Melchinger, "High-throughput non-destructive biomass determination during early plant development in maize under field conditions," *Field Crops Research*, vol. 121, no. 2, pp. 268–273, 2011.
- [27] J. Gai, "Plants detection, localization and discrimination using 3D machine vision for robotic intra-row weed control," Iowa State University, 2016.
- [28] T. Sritarapipat, P. Rakwatin, and T. Kasetkasem, "Automatic rice crop height measurement using a field server and digital image processing," *Sensors*, vol. 14, no. 1, pp. 900–926, 2014.
- [29] M. Mano, "Precise and continuous measurement of plant heights in an agricultural field using a time-lapse camera," *Journal of Agricultural Meteorology*, p. D-16, 2017.
- [30] A. Zehm, M. Nobis, and Angeli. SCHWABE, "Multiparameter analysis of vertical vegetation structure based on digital image processing," *Flora-Morphology, Distribution, Functional Ecology of Plants*, vol. 198, no. 2, pp. 142–160, 2003.
- [31] R. F. Limb, K. R. Hickman, D. M. Engle, J. E. Norland, and S. D. Fuhlendorf, "Digital photography: reduced investigator variation in visual obstruction measurements for southern tallgrass prairie," *Rangeland Ecology & Management*, vol. 60, no. 5, pp. 548–552, 2007.
- [32] O. Tackenberg, "A new method for non-destructive measurement of biomass, growth rates, vertical biomass distribution and dry matter content based on digital image analysis," *Annals of Botany*, vol. 99, no. 4, pp. 777–783, 2007.

- [33] C. Sun, “Study of computer vision method for three dimensional deformation measurement,” Order No. NR59005, Ryerson University, 2009.
- [34] M. Vázquez-Arellano, H. W. Griepentrog, D. Reiser, and D. S. Paraforos, “3-D imaging systems for agricultural applications—a review,” *Sensors (Switzerland)*, vol. 16, no. 5. MDPI AG, 01-May-2016.
- [35] R. Schwarte, G. Häusler, and R. W. Malz, “Three-dimensional imaging techniques,” in *Computer Vision and Applications*, B. Jähne and H. Haußecker, Eds. Academic Press, 2000, pp. 177–208.
- [36] R. Lange, “3D time-of-flight distance measurement with custom solid-state image sensors in CMOS/CCD-technology,” Universitätsbibliothek der Universität Siegen, Adolf-Reichweinstr. 2, 57068 Siegen, 2006.
- [37] D.-I. B. Hagebeuker and P. Marketing, “A 3D time of flight camera for object detection,” *PMD Technologies GmbH, Siegen*, 2007.
- [38] Wikipedia Contributors, “Interferometry,” *Wikipedia, The Free Encyclopedia*, 2019. [Online]. Available: <https://en.wikipedia.org/w/index.php?title=Interferometry&oldid=924892641>. [Accessed: 05-May-2019].
- [39] A. Chaudhury, C. Ward, A. Talasaz, A. Ivanov, M. Brophy, B. Grodzinski, N. Huner, R. Patel, and John L. Barron, “Machine Vision System for 3D Plant Phenotyping,” *IEEE/ACM Transactions on Computational Biology and Bioinformatics*, vol. PP, Apr. 2018.
- [40] S. Sun, C. Li, and A. Paterson, “In-field high-throughput phenotyping of cotton plant height using LiDAR,” *Remote Sensing*, vol. 9, no. 4, p. 377, 2017.
- [41] M. Friedli, N. Kirchgessner, C. Grieder, F. Liebisch, M. Mannale, and A. Walter, “Terrestrial 3D laser scanning to track the increase in canopy height of both

- monocot and dicot crop species under field conditions,” *Plant Methods*, vol. 12, no. 1, p. 9, 2016.
- [42] X. Wang, D. Singh, S. Marla, G. Morris, and J. Poland, “Field-based high-throughput phenotyping of plant height in sorghum using different sensing technologies,” *Plant Methods*, vol. 14, no. 1, p. 53, 2018.
- [43] N. Tilly, D. Hoffmeister, Q. Cao, S. Huang, V. Lenz-Wiedemann, Y. Miao, and G. Bareth, “Multitemporal crop surface models: accurate plant height measurement and biomass estimation with terrestrial laser scanning in paddy rice,” *Journal of Applied Remote Sensing*, vol. 8, no. 1, p. 83671, 2014.
- [44] L. Zhang and T. E. Grift, “A LIDAR-based crop height measurement system for *Miscanthus giganteus*,” *Computers and electronics in agriculture*, vol. 85, pp. 70–76, 2012.
- [45] K. Omasa, F. Hosoi, and A. Konishi, “3D lidar imaging for detecting and understanding plant responses and canopy structure,” *Journal of Experimental Botany*, vol. 58, no. 4, pp. 881–898, Oct. 2006.
- [46] F. Hosoi and K. Omasa, “Estimating vertical plant area density profile and growth parameters of a wheat canopy at different growth stages using three-dimensional portable lidar imaging,” *ISPRS Journal of Photogrammetry and Remote Sensing*, vol. 64, no. 2, pp. 151–158, 2009.
- [47] F. Hosoi, K. Nakabayashi, and K. Omasa, “3-D modeling of tomato canopies using a high-resolution portable scanning lidar for extracting structural information,” *Sensors*, vol. 11, no. 2, pp. 2166–2174, 2011.
- [48] F. Perez-Sanz, P. J. Navarro, and M. Egea-Cortines, “Plant phenomics: an overview of image acquisition technologies and image data analysis algorithms,” *GigaScience*, vol. 6, no. 11, Oct. 2017.

- [49] K. H. Kjaer and C. O. Ottosen, “3D laser triangulation for plant phenotyping in challenging environments,” *Sensors (Switzerland)*, vol. 15, no. 6, pp. 13533–13547, Jun. 2015.
- [50] V. Vadez, J. Kholová, G. Hummel, U. Zhokhavets, S. K. Gupta, and C. T. Hash, “LeasyScan: a novel concept combining 3D imaging and lysimetry for high-throughput phenotyping of traits controlling plant water budget,” *Journal of Experimental Botany*, vol. 66, no. 18, pp. 5581–5593, Jun. 2015.
- [51] C. Bellasio, J. Olejníčková, R. Tesař, D. Šebela, and L. Nedbal, “Computer reconstruction of plant growth and chlorophyll fluorescence emission in three spatial dimensions,” *Sensors*, vol. 12, no. 1, pp. 1052–1071, 2012.
- [52] Y. Li, X. Fan, N. J. Mitra, D. Chamovitz, D. Cohen-Or, and B. Chen, “Analyzing growing plants from 4D point cloud data,” *ACM Transactions on Graphics (TOG)*, vol. 32, no. 6, p. 157, 2013.
- [53] T. Nguyen, D. Slaughter, N. Max, J. Maloof, and N. Sinha, “Structured light-based 3D reconstruction system for plants,” *Sensors*, vol. 15, no. 8, pp. 18587–18612, 2015.
- [54] G. Alenyà, B. Dellen, and C. Torras, “3D modelling of leaves from color and ToF data for robotized plant measuring,” in *2011 IEEE International Conference on Robotics and Automation*, 2011, pp. 3408–3414 (Copyright © 2011; IEEE).
- [55] R. Klose, J. Penlington, and A. Ruckelshausen, “Usability study of 3D time-of-flight cameras for automatic plant phenotyping,” *Bornimer Agrartechnische Berichte*, vol. 69, no. 93–105, p. 12, 2009.
- [56] R. Fernández, C. Salinas, H. Montes, and J. Sarria, “Multisensory system for fruit harvesting robots. Experimental testing in natural scenarios and with different kinds of crops,” *Sensors*, vol. 14, no. 12, pp. 23885–23904, 2014.

- [57] H. Guan, M. Liu, X. Ma, and S. Yu, “Three-dimensional reconstruction of soybean canopies using multisource imaging for phenotyping analysis,” *Remote Sensing*, vol. 10, no. 8, p. 1206, 2018.
- [58] S. Jay, G. Rabatel, X. Hadoux, D. Moura, and N. Gorretta, “In-field crop row phenotyping from 3D modeling performed using Structure from Motion,” *Computers and Electronics in Agriculture*, vol. 110, pp. 70–77, 2015.
- [59] T. Tuong Nguyen, D. C. Slaughter, B. Townsley, L. Carriedo, J. N. N., and N. Sinha, “Comparison of Structure-from-Motion and Stereo Vision Techniques for Full In-Field 3D Reconstruction and Phenotyping of Plants: An Investigation in Sunflower,” *2016 ASABE Annual International Meeting*. ASABE, St. Joseph, MI, p. 1, 2016.
- [60] H. J. Andersen, L. Reng, and K. Kirk, “Geometric plant properties by relaxed stereo vision using simulated annealing,” *Computers and electronics in agriculture*, vol. 49, no. 2, pp. 219–232, 2005.
- [61] R. N. Lati, S. Filin, and H. Eizenberg, “Estimating plant growth parameters using an energy minimization-based stereovision model,” *Computers and Electronics in Agriculture*, vol. 98, pp. 260–271, 2013.
- [62] Y.-H. F. Yeh, T.-C. Lai, T.-Y. Liu, C.-C. Liu, W.-C. Chung, and T.-T. Lin, “An automated growth measurement system for leafy vegetables,” *Biosystems engineering*, vol. 117, pp. 43–50, 2014.
- [63] M. Tilneac, V. Dolga, S. Grigorescu, and M. A. Bitea, “3D stereo vision measurements for weed-crop discrimination,” *Elektronika ir Elektrotechnika*, vol. 123, no. 7, pp. 9–12, 2012.
- [64] F. Apelt, D. Breuer, Z. Nikoloski, M. Stitt, and F. Kragler, “Phytotyping4D: A light-field imaging system for non-invasive and accurate monitoring of spatio-temporal plant growth,” *Plant Journal*, vol. 82, no. 4, pp. 693–706, 2015.

- [65] R. Schima, H. Mollenhauer, G. Grenzdörffer, I. Merbach, A. Lausch, P. Dietrich, and J. Bumberger, “Imagine all the plants: evaluation of a light-field camera for on-site crop growth monitoring,” *Remote Sensing*, vol. 8, no. 10, p. 823, 2016.
- [66] G. Azzari, M. Goulden, and R. Rusu, “Rapid characterization of vegetation structure with a Microsoft Kinect sensor,” *Sensors*, vol. 13, no. 2, pp. 2384–2398, 2013.
- [67] S. Paulus, J. Behmann, A.-K. Mahlein, L. Plümer, and H. Kuhlmann, “Low-cost 3D systems: suitable tools for plant phenotyping,” *Sensors*, vol. 14, no. 2, pp. 3001–3018, 2014.
- [68] M. Hämmerle and B. Höfle, “Direct derivation of maize plant and crop height from low-cost time-of-flight camera measurements,” *Plant Methods*, vol. 12, no. 1, p. 50, 2016.
- [69] N. Lievendag, “3D Scanner alternatives for Microsoft’s Discontinued Kinect,” *3D Scan Expert*. [Online]. Available: <https://3dscanexpert.com/alternatives-microsoft-discontinues-kinect-popular-low-cost-3d-scanner/>. [Accessed: 30-Apr-2019].
- [70] A. Bouvry, “Continuous monitoring of basil (*Ocimum basilicum* L.) topology based on partial 4D point clouds,” Université de Liège, Liège, Belgique, 2017.
- [71] Intel, “Intel® RealSense™ Depth Camera SR300 Series Product Family,” 2019. [Online]. Available: [https://www.intelrealsense.com/wp-content/uploads/2019/07/RealSense\\_SR30x\\_Product\\_Datasheet\\_Rev\\_002.pdf](https://www.intelrealsense.com/wp-content/uploads/2019/07/RealSense_SR30x_Product_Datasheet_Rev_002.pdf). [Accessed: 30-Sep-2019].
- [72] F. Lee, “Choose the Right 3D Vision Camera For Your IoT Device,” *Medium*, 2017. [Online]. Available: <https://medium.com/iotforall/choose-the-right-3d-vision-camera-for-your-iot-device-962d95c581cb>. [Accessed: 21-Apr-2019].
- [73] “Better understand the basics of depth-sensing cameras, and learn how and where



- each class is utilized in the field of augmented reality,” *DAQRI*, 2018. [Online]. Available: <https://daqri.com/blog/depth-cameras-for-mobile-ar/>. [Accessed: 07-Jul-2019].
- [74] S. Liu, D. Gao, P. Wang, X. Guo, J. Xu, and D.-X. Liu, “A Depth-Based Weighted Point Cloud Registration for Indoor Scene,” *Sensors*, vol. 18, no. 11, p. 3608, 2018.
- [75] A. Vit and G. Shani, “Comparing RGB-D Sensors for Close Range Outdoor Agricultural Phenotyping,” *Sensors*, vol. 18, no. 12, p. 4413, 2018.
- [76] “How to Grow Basil,” *Miracle-Gro*. [Online]. Available: [www.miraclegro.com/en-us/library/fruit-vegetable-herb/how-grow-basil](http://www.miraclegro.com/en-us/library/fruit-vegetable-herb/how-grow-basil). [Accessed: 29-Apr-2019].
- [77] T. Sugiura, “Intel RealSense SDK 2 (librealsense2) Sample Program,” 2018. [Online]. Available: [Summary?Blog.unanancyowen.com/en/realsense-sdk-2-samples/](http://Summary?Blog.unanancyowen.com/en/realsense-sdk-2-samples/). [Accessed: 15-May-2019].
- [78] Intel, “librealsense,” 2018. [Online]. Available: <https://github.com/IntelRealSense/librealsense>. [Accessed: 15-May-2019].
- [79] “Computer Vision Toolbox,” *MathWork Documentation*. [Online]. Available: <https://www.mathworks.com/products/computer-vision.html>.
- [80] Intel, “Intel® RealSense™ Camera D400 series Product Family Datasheet,” 2019. [Online]. Available: <https://www.intel.com/content/dam/support/us/en/documents/emerging-technologies/intel-realsense-technology/Intel-RealSense-D400-Series-Datasheet.pdf>. [Accessed: 09-Mar-2019].
- [81] Intel, “Overview of the Intel® RealSense™ Depth Camera D400 Series,” 2019. [Online]. Available: <https://software.intel.com/en-us/realsense/d400>. [Accessed:

15-May-2019].

- [82] “findPointsInROI,” *MathWork Documentation*. [Online]. Available: <https://www.mathworks.com/help/vision/ref/pointcloud.findpointsinroi.html>. [Accessed: 15-May-2019].
- [83] M. Muja and D. G. Lowe, “Fast approximate nearest neighbors with automatic algorithm configuration.,” *VISAPP (1)*, vol. 2, no. 331–340, p. 2, 2009.
- [84] R. B. Rusu, *Semantic 3D object maps for everyday robot manipulation*. Springer, 2013.
- [85] R. B. Rusu, Z. C. Marton, N. Blodow, M. Dolha, and M. Beetz, “Towards 3D point cloud based object maps for household environments,” *Robotics and Autonomous Systems*, vol. 56, no. 11, pp. 927–941, 2008.
- [86] T. Opsahl, “Robust estimation with RANSAC,” *University of Oslo*. [Online]. Available: [https://www.uio.no/studier/emner/matnat/its/nedlagte-emner/UNIK4690/v16/forelesninger/lecture\\_3\\_3-robust-estimation-with-ransac.pdf](https://www.uio.no/studier/emner/matnat/its/nedlagte-emner/UNIK4690/v16/forelesninger/lecture_3_3-robust-estimation-with-ransac.pdf). [Accessed: 15-Mar-2019].
- [87] M. A. Fischler and R. C. Bolles, “Random sample consensus: a paradigm for model fitting with applications to image analysis and automated cartography,” *Communications of the ACM*, vol. 24, no. 6, pp. 381–395, 1981.
- [88] K. Olofsson, J. Holmgren, and H. Olsson, “Tree Stem and Height Measurements using Terrestrial Laser Scanning and the RANSAC Algorithm,” *Remote Sensing*, vol. 6, no. 5, pp. 4323–4344, May 2014.
- [89] R. Kurban, F. Skuka, and H. Bozpolat, “Plane Segmentation of Kinect Point Clouds using RANSAC,” in *7th International Conference on Information Technology*, 2015, pp. 545–551.

- [90] L. Li, F. Yang, H. Zhu, D. Li, Y. Li, and L. Tang, "An improved RANSAC for 3D point cloud plane segmentation based on normal distribution transformation cells," *Remote Sensing*, vol. 9, no. 5, p. 433, 2017.
- [91] R. Schnabel, R. Wahl, and R. Klein, "Efficient RANSAC for Point-Cloud Shape Detection," *Computer Graphics Forum*, vol. 26, no. 2, pp. 214–226, Jun. 2007.
- [92] P. H. S. Torr and A. Zisserman, "MLE-SAC: A new robust estimator with application to estimating image geometry," *Computer vision and image understanding*, vol. 78, no. 1, pp. 138–156, 2000.
- [93] J. King, "Dot Product and Normals to Lines and Plane." [Online]. Available: <http://sites.math.washington.edu/~king/coursedir/m445w04/notes/vector/normals-planes>. [Accessed: 15-May-2019].
- [94] Wikipedia contributors, "Rotation matrix," *Wikipedia, The Free Encyclopedia*, 2019. [Online]. Available: [https://en.wikipedia.org/wiki/Rotation\\_matrix](https://en.wikipedia.org/wiki/Rotation_matrix). [Accessed: 29-Apr-2019].
- [95] W. Yang, S. Wang, X. Zhao, J. Zhang, and J. Feng, "Greenness identification based on HSV decision tree," *Information Processing in Agriculture*, vol. 2, no. 3–4, pp. 149–160, 2015.
- [96] H. Wang and D. Suter, "Color image segmentation using global information and local homogeneity," in *Proceeding of 7th Conf. of Digital Image Computing: Techniques and Applications*, 2003.
- [97] K. H. Bin Ghazali, J. Ma, and R. Xiao, "Driver's face tracking based on improved CAMSHIFT," *International Journal of Image, Graphics and Signal Processing*, vol. 5, no. 1, p. 1, 2013.
- [98] W. Contributors, "HSL and HSV," *Wikipedia, The Free Encyclopedia*, 2019. [Online]. Available:

[https://en.wikipedia.org/w/index.php?title=Special:CiteThisPage&page=HSL\\_and\\_HSV&id=917313491](https://en.wikipedia.org/w/index.php?title=Special:CiteThisPage&page=HSL_and_HSV&id=917313491). [Accessed: 20-Oct-2019].

- [99] A. R. Smith, “Color gamut transform pairs,” *ACM Siggraph Computer Graphics*, vol. 12, no. 3, pp. 12–19, 1978.

## Appendices

## Curriculum Vitae

**Name:** Leila Bahman

**Post-secondary Education and Degrees:** Islamic Azad University of Najafabad  
Najafabad, Isfahan, Iran  
2000-2004 BSc.

The University of Western Ontario  
London, Ontario, Canada  
2017-2019 MSc.

**Honours and Awards:** MITACS Accelerate Internship award  
2017,2018

**Related Work Experience** Graduate Research Assistant  
The University of Western Ontario  
2017-2019

**Publications:**